ANL/FE-89/7

High-Temperature Oxidation and Sulfidation of Fe-20Cr-16Ni-4Al-1Y_2O_3 Oxide-Dispersion-Strengthened Alloy

by A. U. Malik and K. Natesan

Argonne National Laboratory, Argonne, Illinois 60439
operated by The University of Chicago
for the United States Department of Energy under Contract W-31-109-Eng-38

This report has been reproduced from the best available copy.

Available from the
National Technical Information Service
U.S. Department of Commerce
5285 Port Royal Road
Springfield, VA 22161

Price: Printed Copy A03
Microfiche A01

Distribution Category:
Coal-Based Materials
and Components (UC-114)

ANL/FE--89/7

DE90 007897

ANL/FE-89/7

ARGONNE NATIONAL LABORATORY
9700 South Cass Avenue
Argonne, Illinois 60439

HIGH-TEMPERATURE OXIDATION AND SULFIDATION OF Fe–20Cr–16Ni–4Al–1Y_2O_3 OXIDE-DISPERSION-STRENGTHENED ALLOY

by

A. U. Malik* and K. Natesan

Materials and Components Technology Division

October 1989

Prepared for
U.S. Department of Energy, Office of Fossil Energy, Advanced Research and Technology Development (AR&TD) Materials Program

*On visiting appointment from Aligarh Muslim University, Aligarh, India.

CONTENTS

FIGURES

TABLES

HIGH–TEMPERATURE OXIDATION AND SULFIDATION OF Fe–20Cr–16Ni–4Al–1Y_2O_3 OXIDE–DISPERSION–STRENGTHENED ALLOY

by

A. U. Malik and K. Natesan

ABSTRACT

High–temperature oxidation and sulfidation studies were conducted on an oxide–dispersion–strengthened alloy of composition Fe-20Cr-16Ni-4Al-1Y_2O_3. The oxidation studies were conducted in air and low-pO_2 environments over a temperature range of 650 to 1200°C. Results are also reported on the sulfidation resistance of preformed oxide scales and the influence of reoxidation of preformed sulfide scales. Detailed microstructural results and X-ray diffraction analysis data are presented to substantiate the corrosion behavior of the alloy over the wide range of conditions anticipated in fossil-energy systems. Data are also presented on the corrosion behavior of the alloy in oxygen/sulfur mixed gas atmospheres, and the results are used to compare the corrosion behavior of the present alloy with other chromia- and alumina-forming alloys.

INTRODUCTION

Profound interest has been shown in recent years in the development of oxide-dispersion-strengthened (ODS) alloys for their exceptional creep resistance, high strength, and oxidation resistance at elevated temperatures. The mechanism of dispersion strengthening with suitable stable oxide particles offers the possibility of increasing the high–temperature strength of corrosion–resistant alloys without an associated loss in surface stability. The surface stability may include resistance to oxidation, sulfidation, and attack by molten salts or ash. These processes are encountered in many industrial operations such as the processing of glass and refractory ceramics, and in furnace atmospheres and gas turbine engines.

Extensive literature[1-4] is available on the preparation of ODS alloys. The techniques of mechanical alloying and hot extrusion of powders are employed for the fabrication of oxide–dispersed alloys. The powder metallurgical technique has been used to achieve optimum properties in a range of commercial alloys such as MA 6000, MA 754, and MA 956. Among ODS superalloys, the Ni-base alloy Ni-20Cr-2ThO_2 (designated by the trade name TD-NiCr) is perhaps the oldest and best

known. The alloy has good oxidation resistance and is used in advanced jet engines and in the thermal protection system for the NASA space shuttle.[5]

Commercially available heat–resisting alloys are classified into two broad families, namely, ferritic and austenitic, depending on their crystal structure. The ferritic Fe-Cr-Al alloys, in addition to their lower raw material cost and generally superior oxidation resistance, have a higher melting point, lower density and a lower coefficient of thermal expansion than the Ni- and Co-base alloys. However, their body-centered cubic structure renders them mechanically weak and provides poor creep resistance and a strong susceptibility to low–temperature brittleness. The more ductile and more creep–resistant austenitic Fe-Cr-Ni-Al alloys owe their ability to withstand high–temperature oxidation chiefly to their development of adherent oxide scales.

A considerable number of papers have been published over the past 15 years on the influence of oxide dispersions on the oxidation/corrosion resistance of Ni-, Co-, and Fe-base alloys. The presence of Y_2O_3 dispersion in Cr-containing Ni- and Co-base alloys results in reduced oxidation rates and greater adhesion of Cr_2O_3. In dispersoid–containing alloys, the scale-forming reaction occurs at the scale/metal interface, while in dispersion-free alloys, the reaction occurs at the scale/gas interface. Improvement is much more pronounced in Co-base alloys in which the scales are prone to spallation in the absence of dispersion.[6] The high–temperature oxidation of Ni-Cr alloys containing various oxides (Y_2O_3, La_2O_3, Al_2O_3, TiO_2, MgO, or SiO_2) showed that the oxidation rate is dependent on the type of the dispersoid.[7] The dispersion of rare earth oxides suppressed the spalling of scales, whereas additions of MgO or SiO_2 accelerated it. The influence of applied Ca, Ce, Hf, La, Y, or Zr nitrate, converted into oxides, on the oxidation behavior of Co- and Ni-base alloys at 1000°C in 1 atm O_2 was very minimal for non-Cr_2O_3–forming alloys.[8] The effect on Cr_2O_3-forming alloys varies with the reactive element. This behavior is associated with the tendency of the reactive element to form small oxide particles on the alloy surface. When these particles are formed effectively, as in the case of La-, Y-, and Ce-oxides, the effects are most dramatic and appear to be similar to those observed when dispersions of reactive element oxides are present within the alloy; however, the beneficial effect does not seem long–lasting. Luthra and Hall[9] conducted high–temperature oxidation studies on plasma–sprayed coatings of Ni-20Cr-12.5Al containing 1 wt.% of MgO, La_2O_3, or Y_2O_3, or 0.8 wt.% Y. Based on cyclic tests conducted at 1150 and 1250°C, they concluded that the coating with 1 wt.%Y_2O_3 had the best oxidation resistance.

High–temperature oxidation studies conducted on Fe-base alloys containing oxide dispersoids generally reveal improvements in terms of scale adherence and oxidation resistance when compared with those without dispersoids.[2,10,11] In a typical case represented by Fe-20Ni-25Cr-5Al-Y alloy, the alumina scales contain a

certain amount of spinel, and Y enters via solid solution in the alumina layer, which seems responsible for improved adherence of the scales.[12] A study on the effect of doping on the oxidation behavior of ferritic Fe-6Al-M and austenitic Fe-27Ni-4Al-M alloys (where M = Ti, Zr,V,Nb,W,B,Si) in H_2/H_2O atmospheres (pO_2 = 10 bar) at 1000°C shows badly adherent scale layers with most of the dopants.[13] However, on alloys with additions of 0.1 to 1.0 wt.% Ti, Zr, V or Y, the oxide layers are fine–grained and adhere well. Ti-doped alloys show very protective layers due to the formation of a Ti(C,O) layer beneath the α-alumina.

There are several theories to explain the beneficial role of rare earths, other reactive elements, or dispersion of stable oxides in greatly improving the high–temperature oxidation resistance of alloys. Whittle and Stringer[14] extensively reviewed the earlier studies on the subject and discussed at length the merits and drawbacks of various theories/models. Two major effects induced by the reactive elements or dispersion of stable oxides are improved adhesion between the scale and the substrate (which leads to better corrosion resistance under thermal cycling conditions) and, in some cases, reduction of the actual growth rate of the oxide. Of the various models, the most significant are based on mechanical keying of the surface scale to the substrate by the formation of intrusions of oxide penetrating into the alloy and the elimination of void formation at the alloy/scale interface. Hindam and Whittle,[15] while investigating oxidation-induced growth of a peg-like morphology in Ni and Fe alloys containing oxygen-active additions, identified two types of pegs. Classical internal oxidation theory or a short–circuit model was used to explain the development of pegs. Ramanarayanan et al.[16] studied the characteristics of alumina scales formed on Fe-20Cr-4.5Al-0.5Ti-0.5Y_2O_3. It is suggested that the remarkable adherence of the alumina scales is a consequence of a combination of factors. First, Y doping promotes the development of a fine grained α-alumina scale that can effectively relieve oxide growth stresses by diffusional plastic flow. Second, because the alumina scale grows by exclusive inward oxygen transport, growth stresses arising from alumina nucleation within an existing scale are avoided.

Smeggil et al.[17] proposed an entirely new mechanism to account for the beneficial effects that small additions of elements such as Y have on the adherence of oxide scales. It is well known that sulfur in Ni- or Ni-base alloys, even in trace levels, weakens the bond between the protective scale and the substrate due to segregation of sulfur. The role of Y is to interact with indigenous sulfur in the alloy to form a sulfide phase that lessens the amount of sulfur available for segregation at the scale/metal interface. If this mechanism is operative for the improved oxidation resistance of alloys that contain a rare-earth element, it will be a cause for concern that these alloys will not exhibit adequate resistance to oxidation-sulfidation attack when exposed to sulfur-containing bioxidant environments. The major reasons for this expectation are that the alloys generally contain a very small

amount (in the range of 0.5 to 1.0 wt.%) of the rare-earth element and that a substantial source for sulfur is always present in the exposure environment.

This report describes the experimental data developed on an Fe-base ODS alloy exposed to oxidizing and/or sulfidizing environments. Detailed information is presented on the microstructures and chemical compositions of the corrosion-product layers that developed under various exposure conditions. The data are used to assess the role, if any, of the rare earth oxide addition in the oxidation/sulfidation behavior of the alloy.

EXPERIMENTAL PROCEDURE

Material Preparation

Pure powders of Fe, Cr, Ni, Al, and dispersoids were mixed and ball–milled in a high–energy attritor in an argon atmosphere to produce alloy powders. The chemical compositions of the pure powders, alloy powder, and alloy sheet are given in Table 1. The alloy with Y_2O_3 dispersion was ball–milled for 20.75 h, and intermediate samplings of the powders were made at 7 and 15.3 h. The particle size of the attrited alloy powder was in the range of 125 to 177 μm. Additional details on the fabrication of ODS alloys have been reported elsewhere.[18] Analysis of the alloy powder, using a scanning electron microscope, indicated a uniform distribution of Fe, Cr, Ni, and Al in the attrited alloy. The dispersoid concentration was below the detectibility limit of the energy–dispersive X-ray analyzer. The alloy powder was canned in a stainless steel container with a backfill of argon gas and consolidated by extrusion at 1000°C. The extruded rods were rolled into sheets, and corrosion test coupons of 10 x 5 x 0.5 mm were cut from the sheets. The specimen faces were polished with 600–grit SiC paper and cleaned ultrasonically in acetone. The alloy samples were vacuum–annealed at 1050°C for about 6 h.

Oxidation Experiments

The oxidation experiments were performed using an electrobalance, made by CAHN Instruments, Inc., that had a sample capacity of 2.5 g and a sensitivity of 0.1 μg. The weighing mechanism was enclosed in glass assemblies that isolated the reaction gas mixture from the balance mechanism. Helium gas flowed through the balance assembly countercurrent to the reaction gas mixture that flowed in the furnace chamber. The reaction chamber was connected to the balance assembly by a ~300–mm–long Pyrex tube. The bottom portion of the reaction chamber was filled with glass balls that mixed and preheated the incoming reaction gas mixture before exposure to the specimens. The furnace consisted of three-zone Kanthal heating elements with a temperature capability of 1200°C in continuous operation.

Table 1. Chemical Composition of Pure Powders, Alloy Powder, and Sheet Specimens of ODS Material (wt.%)

Material	C	N	S	Mn	Ni	Cr	Al	Mo	Cu	Pb	V	Co	Fe	Other
Chromium	0.017	0.0124	0.021	0.01	<0.01	Bal.	<0.01	<0.01	<0.01	0.02	<0.01	0.01	–	–
Nickel	0.08	0.0234	0.004	<0.01	Bal.	0.04	<0.01	<0.01	<0.01	<0.01	<0.01	<0.01	–	–
Iron	0.010	0.0160	0.015	0.07	0.03	0.01	<0.01	<0.01	<0.03	<0.01	<0.01	0.01	Bal.	–
Aluminum	0.022	–	0.003	<0.01	<0.01	<0.01	Bal.	0.01	<0.01	<0.01	<0.01	0.03	–	–
Y_2O_3	0.08	<0.001	0.079	<0.01	0.01	<0.01	<0.01	<0.01	<0.01	<0.01	<0.01	<0.01	–	Y_2O_3 Bal.
Alloy Powder	0.15	0.0231	0.012	0.06	16.40	18.92	3.89	0.02	0.03	<0.01	<0.01	0.01	Bal.	Rare Earth 1.45
Alloy Sheet	0.17	0.0235	0.015	0.05	15.60	18.78	4.42	0.02	0.03	–	–	–	59.02	Si 0.02, P 0.010, RE 1.71

The test specimens were suspended from the balance with a ~200–μm–diameter platinum wire. The tests were started by setting up the specimen at room temperature and purging the system with the appropriate reaction gas mixture. The specimen was heated in the reaction gas to the desired test temperature. Upon completion of the test, the furnace was opened and the specimen was cooled rapidly in the reaction gas environment. The oxidation and sulfidation kinetic studies were conducted at temperatures of 650, 871, 1000, and 1200°C. The exposure environments used for the oxidation studies were oxygen, air, 1 vol.% CO-CO_2, and 45 vol.% CO-45 vol.% CO_2-10 vol.% CH_4; those for sulfidation were H_2/H_2S gas mixtures with several levels of H_2S content. Several experiments were also conducted in two different oxygen/sulfur mixed gas environments to compare the corrosion behavior of the present alloy with the data developed earlier for other candidate alloys.[19,20] Calculated values for the oxygen and sulfur partial pressures established by different exposure environments are listed in Table 2. In addition, a few oxidation tests were conducted to evaluate the effects, if any, of the surface preparation on oxidation rate and morphology of the oxide scales. Further, a number of preoxidation/sulfidation and presulfidation/oxidation tests were performed to examine the sulfidation resistance of the oxide scale and the reformability of the oxide scale in a sulfidized alloy.

Upon completion of the kinetic runs, the morphology and structure of the oxide/sulfide scales formed on the alloy surface were examined by optical metallography, scanning electron microscopy, X-ray diffraction analysis, electron dispersion X-ray analysis (EDAX), and electron probe microanalysis (EPMA).

RESULTS

Oxidation Tests

Figures 1–3 show thermogravimetric test data for the oxidation of the ODS alloy at 1200, 1000, and 650°C, respectively, after exposure to several oxidizing environments. Figures 4–6 show the same data plotted as the square of the weight change versus exposure time. The linear behavior of the data in these plots indicates that the oxidation process follows parabolic kinetics. Table 3 lists the values of the parabolic rate constant, k_p, calculated from the data at several temperatures and exposure environments. As expected, the value of k_p increases with an increase in exposure temperature. Figure 7 represents an Arrhenius plot (log k_p versus reciprocal temperature) for the oxidation of the alloy in different environments. The plots are not particularly linear and there appears to be an abnormal increase in the oxidation rate as the temperature increases from 1000 to 1200°C, possibly due to vapor–phase loss of chromium and volatile chromium oxide. The results also indicate no monotonic dependence of the oxidation rate on the oxygen partial pressure in the exposure environment.

Table 2. Calculated Values for Oxygen and Sulfur Partial Pressures in Various Gas Mixtures and at Temperatures Used in Experimental Program (atm)

Exposure Environment	pO_2				pS_2			
	650°C	871°C	1000°C	1200°C	650°C	871°C	1000°C	1200°C
Oxygen	1.0	1.0	1.0	1.0	–	–	–	–
Air	0.21	0.21	0.21	0.21	–	–	–	–
1 CO–CO_2	1.2×10^{-19}	1.9×10^{-13}	7.6×10^{-11}	1.1×10^{-7}	–	–	–	–
45 CO–45 CO_2–10 CH_4	1.5×10^{-23}	3.0×10^{-18}	1.1×10^{-15}	1.2×10^{-12}	–	–	–	–
0.162 H_2S–H_2	–	–	–	–	2.2×10^{-11}	2.1×10^{-9}	1.5×10^{-8}	1.6×10^{-7}
0.35 H_2S–H_2	–	–	–	–	1.0×10^{-10}	1.0×10^{-8}	7.1×10^{-8}	7.8×10^{-7}
1.35 H_2S–H_2	–	–	–	–	1.5×10^{-9}	1.5×10^{-7}	1.1×10^{-6}	1.1×10^{-5}
O/S Mixed Gas 1	1.2×10^{-23}	4.2×10^{-18}	1.2×10^{-15}	1.2×10^{-12}	4.6×10^{-10}	4.1×10^{-8}	3.5×10^{-7}	4.2×10^{-6}
O/S Mixed Gas 2	1.2×10^{-23}	4.1×10^{-18}	1.2×10^{-15}	1.1×10^{-12}	1.1×10^{-8}	9.4×10^{-7}	8.0×10^{-6}	9.2×10^{-5}

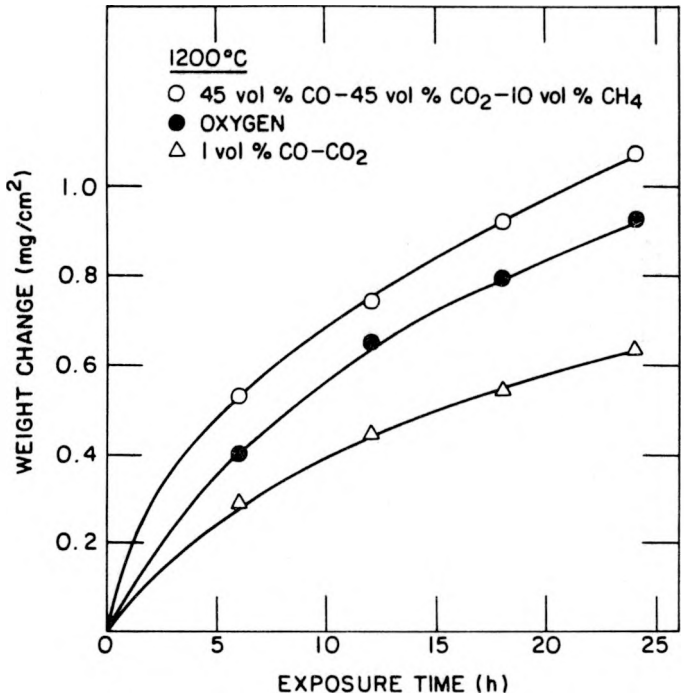

Fig. 1. Thermogravimetric Test Data for Oxidation of ODS Alloy at 1200°C.

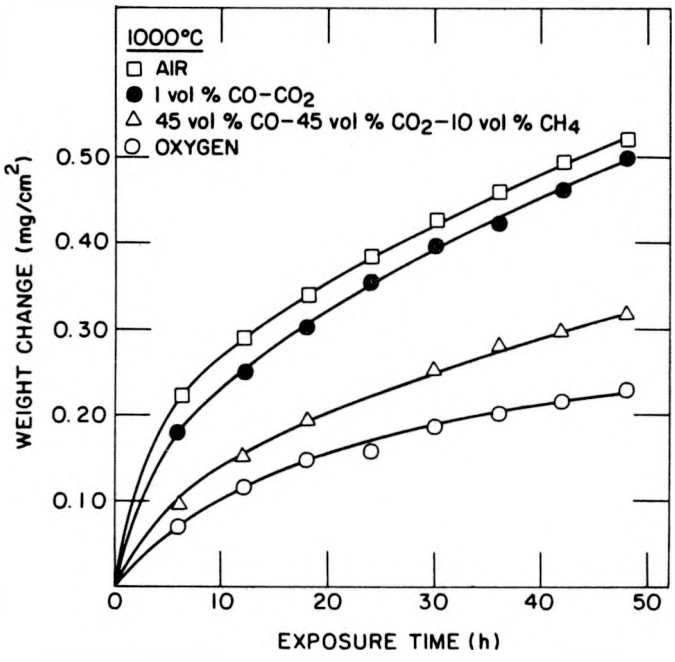

Fig. 2. Thermogravimetric Test Data for Oxidation of ODS Alloy at 1000°C.

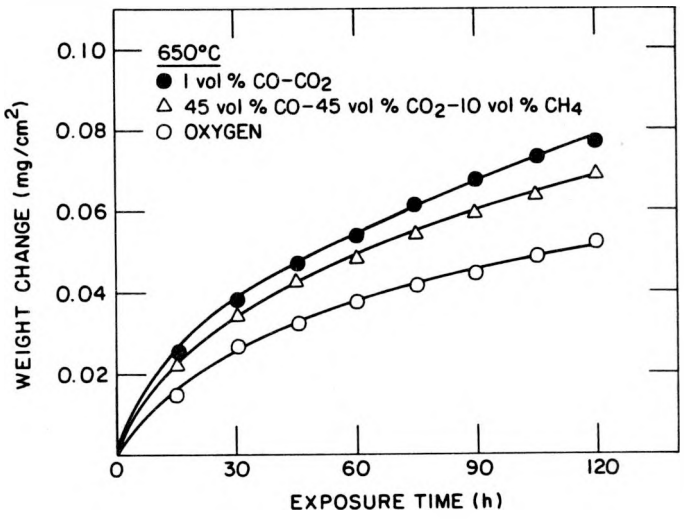

Fig. 3. Thermogravimetric Test Data for Oxidation of ODS Alloy at 650°C.

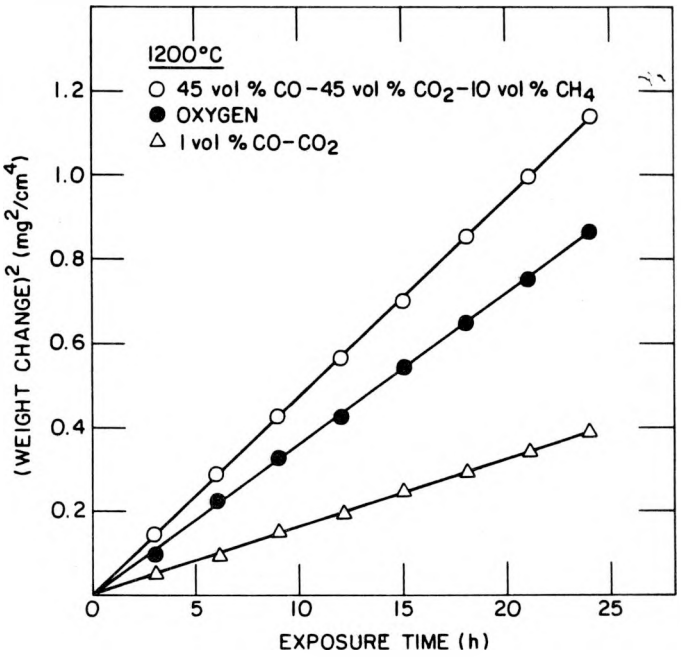

Fig. 4. Plot of Square of Weight Change Data versus Time for Oxidation of ODS Alloy at 1200°C.

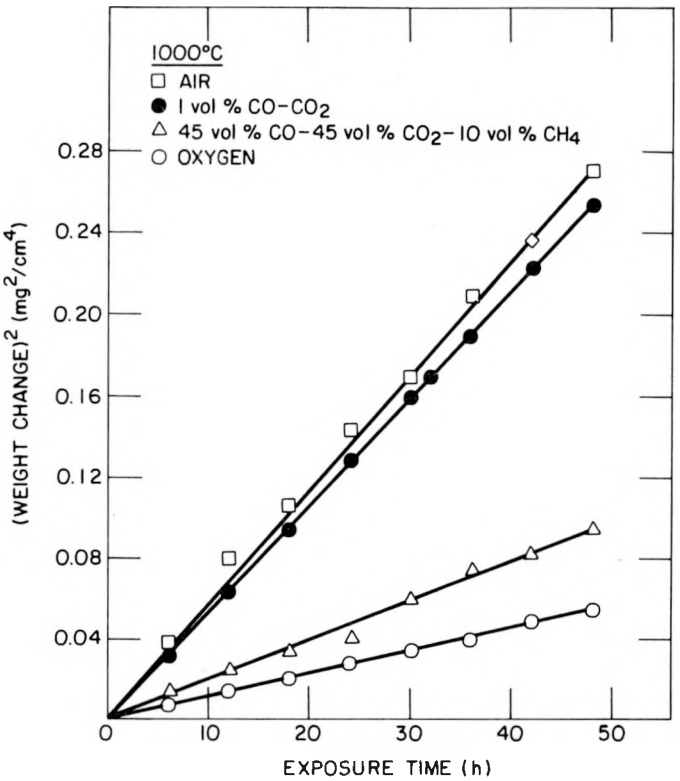

Fig. 5. Plot of Square of Weight Change Data versus Time for Oxidation of ODS Alloy at 1000°C.

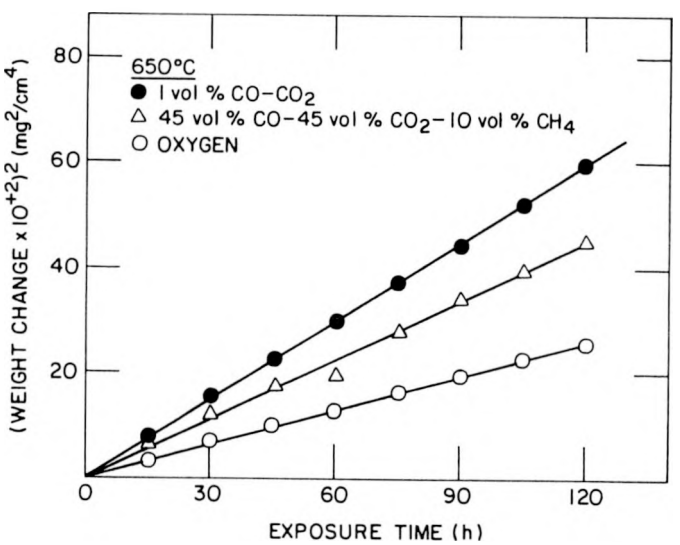

Fig. 6. Plot of Square of Weight Change Data versus Time for Oxidation of ODS Alloy at 650°C.

Table 3. Parabolic Rate Constant, k_p, for Oxidation of ODS Alloy under Different Test Conditions

Temp. (°C)	Exposure Environment	k_p ($mg^2\ cm^{-4}\ s^{-1}$)
650	O_2	5.9×10^{-9}
	45 CO–45 CO_2–10 CH_4	8.9×10^{-9}
	1 CO–CO_2	1.4×10^{-8}
1000	O_2	3.1×10^{-7}
	45 CO–45 CO_2–10 CH_4	5.5×10^{-7}
	1 CO–CO_2	1.5×10^{-6}
	Air	1.6×10^{-7}
1200	O_2	1.0×10^{-5}
	45 CO–45 CO_2–10 CH_4	1.3×10^{-5}
	1 CO–CO_2	2.8×10^{-5}

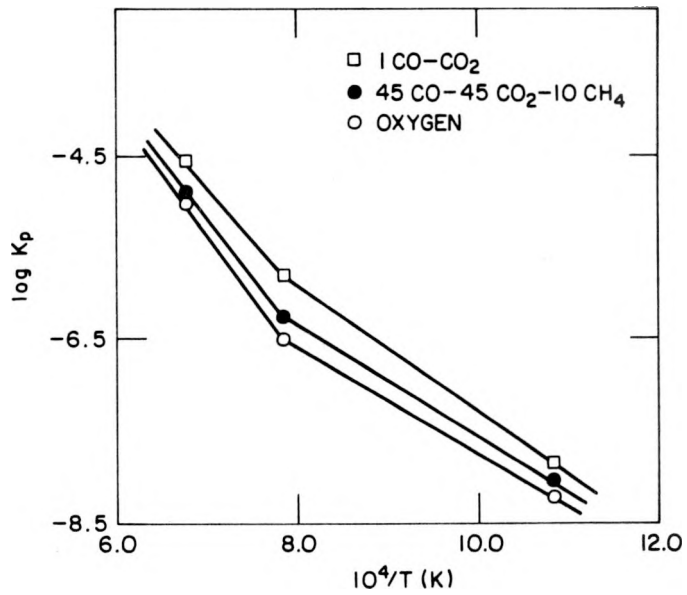

Fig. 7. Temperature Dependence of Parabolic Rate Constant for Oxidation of ODS Alloy.

Effect of surface finish on the oxidation behavior of the ODS alloy was studied using samples polished on 320–grit SiC paper and after electropolish and grit-blast operations. Figure 8 shows weight change versus time plots for specimens with different surface treatments. The results show that the weight gain for the grit-blasted sample was substantially larger than those for the other two treatments. For example, after 12 h oxidation at 1000°C in 45 vol.% CO-45 vol.% CO_2-10 vol.% CH_4 gas, the weight gain for the grit-blasted sample was ~4.2 mg/mm^2, while that for the electropolished and SiC–abraded samples was 0.2 mg/mm^2.

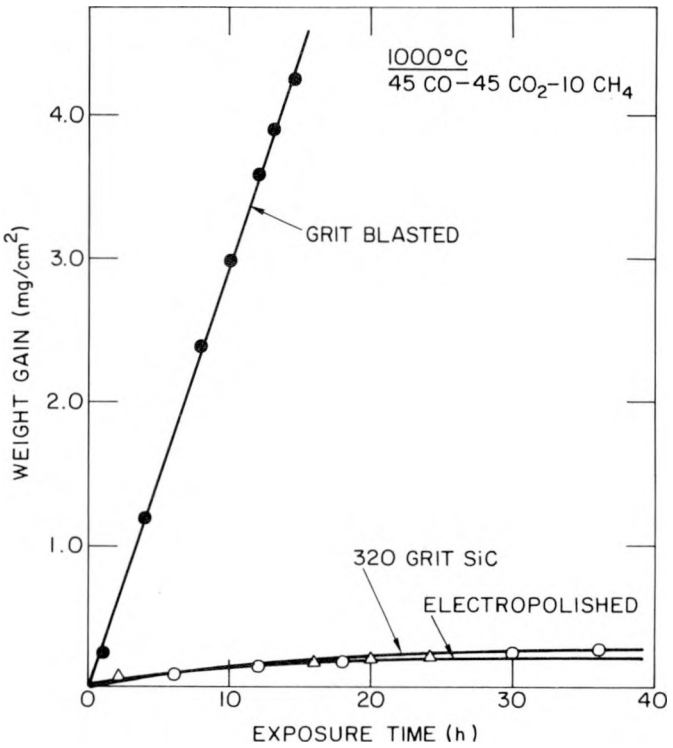

Fig. 8. Effect of Initial Surface Treatment on Oxidation Kinetics of ODS Alloy at 1000°C.

Morphology of Oxidized Alloys

The microstructures of the ODS alloy in the as–cast, grit–blasted, and annealed conditions consisted of a two-phase mixture of Ni_3Al and Fe-rich matrix. The volume fraction of Y_2O_3 particles was too small to detect with an electron microprobe. While the as–cast and grit–blasted specimens contained fine particles of Ni_3Al, the annealed sample had a coarse–grained and more homogeneous structure.

Figure 9 shows SEM photographs of ODS alloy cross sections after exposure at 1000°C to oxygen, air, and low-pO_2 environments. The scale thicknesses in all cases were extremely small and consisted of α-alumina. Figure 10 shows EDAX spectra

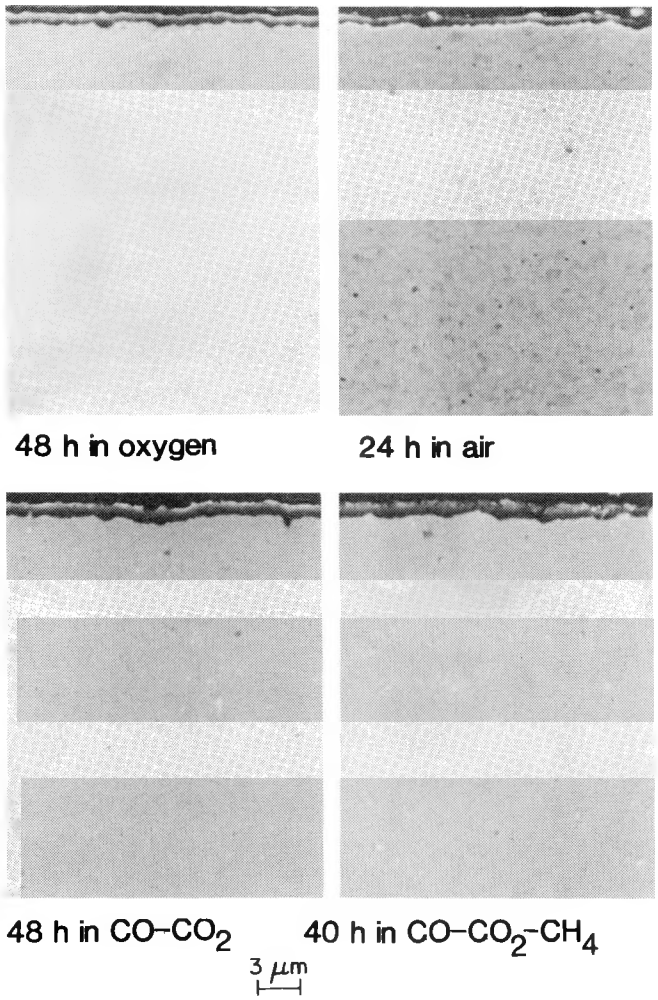

Fig. 9.
SEM Photographs of Cross Sections of ODS Alloy Specimens after Exposure to Various Oxidizing Environments at 1000°C.

for specimen surfaces after exposure to various conditions. The scales developed at 1000°C were predominantly alumina. Diffraction analysis also showed Ni3Al precipitates in all oxidized specimens. The data show that even at 650°C, the alloy developed an almost pure alumina scale; however, at this temperature the scale thickness was extremely small (~0.1 μm) after 131 h exposure. Table 4 lists the phases identified by X-ray diffractometer analysis of specimens after exposure in oxidizing atmospheres. In addition to X-ray diffractometer analysis of "in-situ" scales, the oxide scales were scraped from the oxidized surfaces and analyzed with the Debye Scherrer powder method. The results were consistent with those developed using an X-ray diffractometer.

Figure 11 shows SEM photographs of the alloy after exposure to different oxidizing environments at 1200°C. The oxide thicknesses at 1200°C were somewhat larger than those developed at 1000°C, and the diffraction analysis indicated the presence of chromia in the scale, as well as $FeCr_2O_4$ and $NiO.Cr_2O_3$ phases. EPMA analysis also showed the presence of Y in the scale at a much higher concentration (~3.5 wt.%) than that present in the matrix (0.6 wt.%). The analysis also showed the

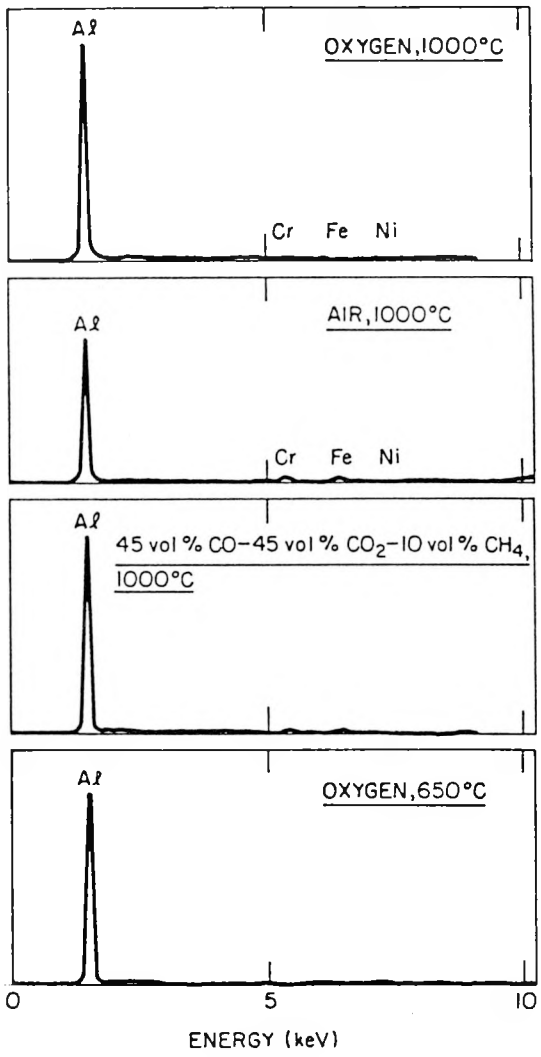

Fig. 10.
EDAX Spectra for Oxide Scales Developed after Exposure to Various Oxidizing Environments.

presence of Y in much higher concentration at the alloy/scale interface than in the matrix. Figure 12 shows SEM photographs and EDAX spectra for different regions of scale in a grit–blasted specimen after exposure in CO-CO_2-CH_4 gas mixture for 60 h at 1000°C. The specimen developed a multilayered scale that consisted of an outer layer of Cr_2O_3 and $FeCr_2O_4$ and an inner layer of alumina. Figure 13 shows similar information for an electropolished specimen exposed for 40 h to conditions identical to that for grit–blasted specimens. The scale in this case was very thin and consisted predominantly of alumina, which appeared much more protective than the scale in the grit–blasted specimen.

Sulfidation, Oxidation/Sulfidation, and Sulfidation/Oxidation Tests

Figure 14 shows thermogravimetric test data for the sulfidation of the ODS alloy exposed to two sulfur–containing gas mixtures at 1000°C. The observed sulfidation rates are linear, and the linear rate constants (k_ℓ) for sulfidation are at least three orders of magnitude higher than the parabolic rate constants obtained for

Table 4. X–Ray Diffractometer Analysis of ODS Alloy Specimens after Oxidation

Oxidation Atmosphere	Temp. (°C)	Reaction Phases Identified	
		Major	Minor
1 CO–CO_2	650	Ni_3Al, αAl_2O_3	–
	1000	Ni_3Al, αAl_2O_3	$FeCr_2O_4$, $NiO.Cr_2O_3$
	1200	Ni_3Al, αAl_2O_3, Cr_2O_3	$FeCr_2O_4$, $NiO.Cr_2O_3$
O_2	1000	Ni_3Al, αAl_2O_3	–
	1200	Ni_3Al, αAl_2O_3	–
CO–CO_2–CH_4	1000	Ni_3Al, αAl_2O_3	$FeCr_2O_4$, $NiO.Cr_2O_3$
	1200	Ni_3Al, αAl_2O_3	$FeCr_2O_4$, $NiO.Cr_2O_3$
	1000	Cr_2O_3[a]	$FeCr_2O_4$, $NiO.Cr_2O_3$

[a]Grit–blasted specimen.

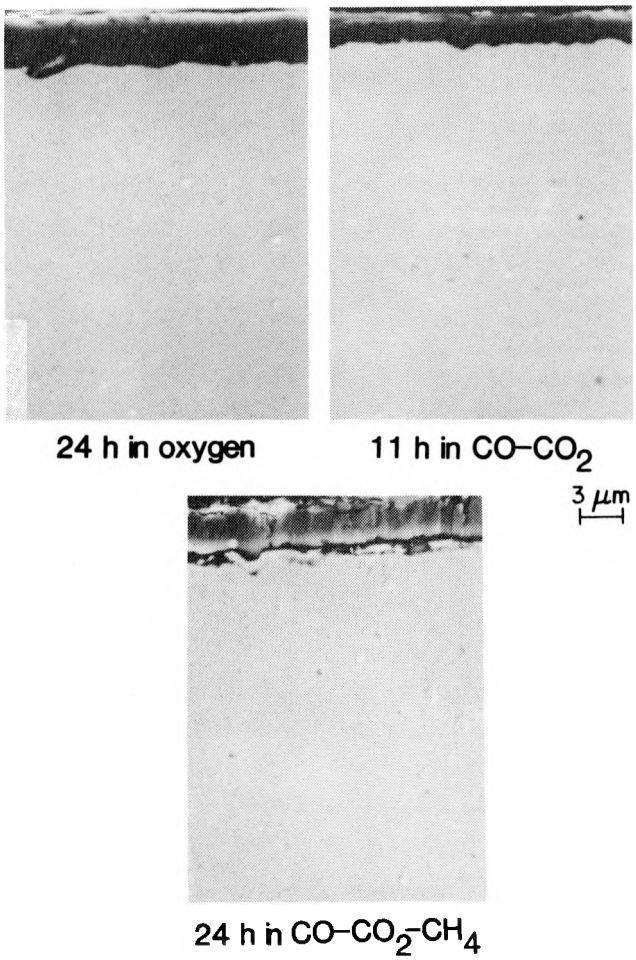

Fig. 11.
SEM Photographs of Cross Sections of ODS Alloy Specimens after Exposure to Various Oxidizing Environments at 1200°C.

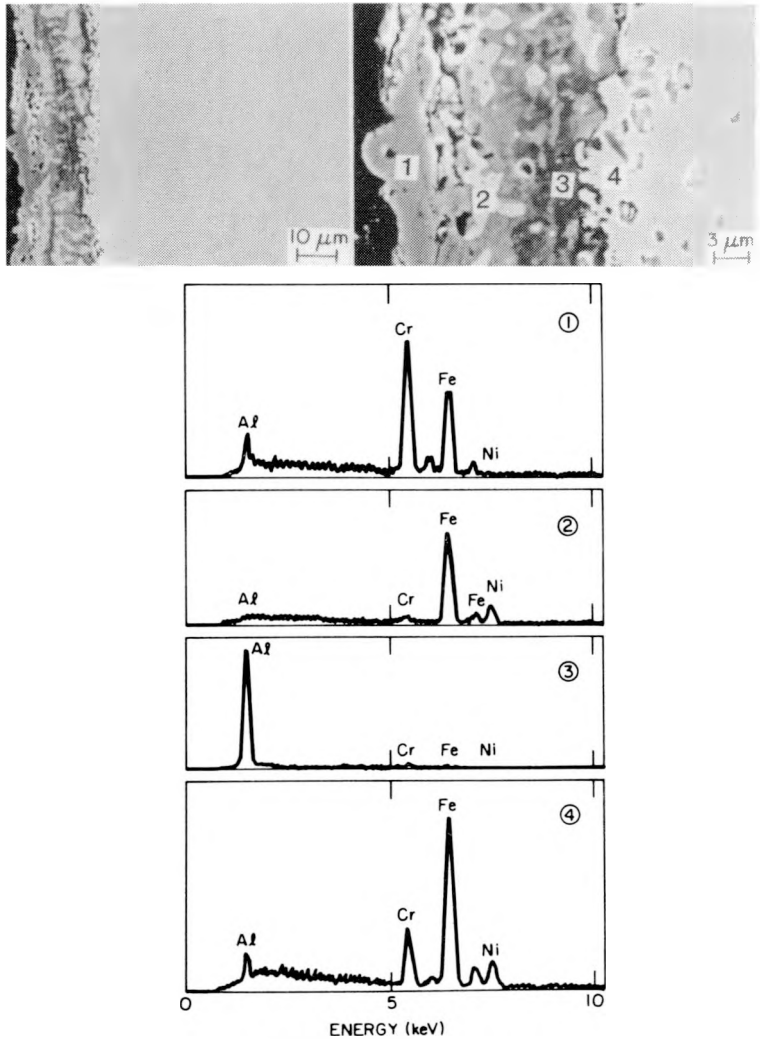

Fig. 12. EDAX Analysis of Different Regions of Scale Developed on Grit-Blasted Specimen after Exposure in CO–CO_2–CH_4 Gas Mixture at 1000°C.

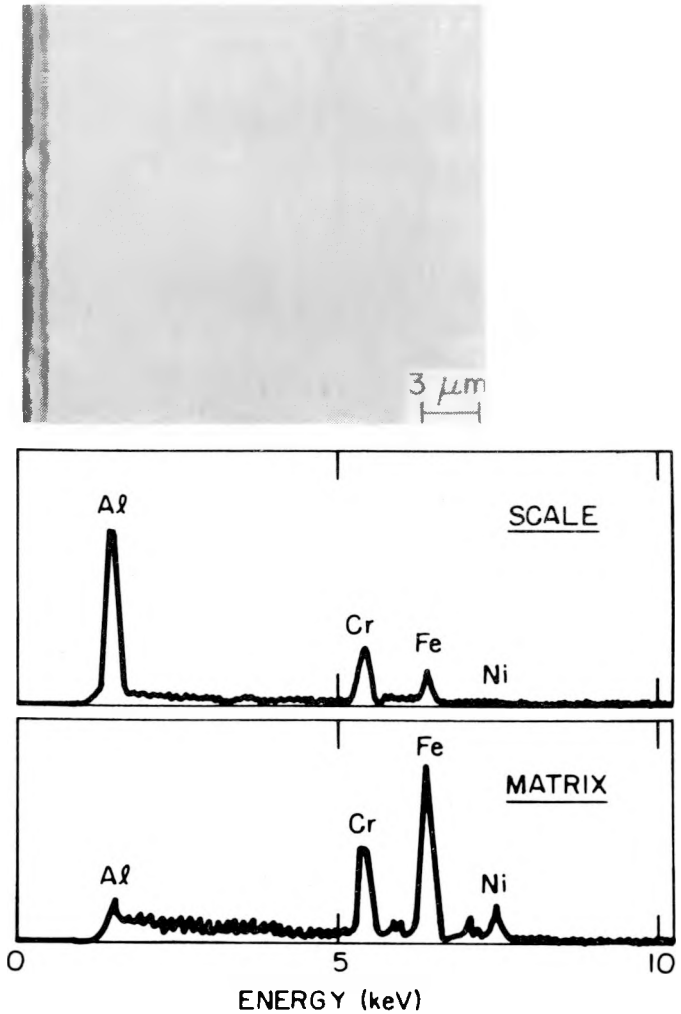

Fig. 13. EDAX Analysis of Scale and Substrate Alloy for Electropolished Specimen after Exposure in CO–CO_2–CH_4 Gas Mixture at 1000°C.

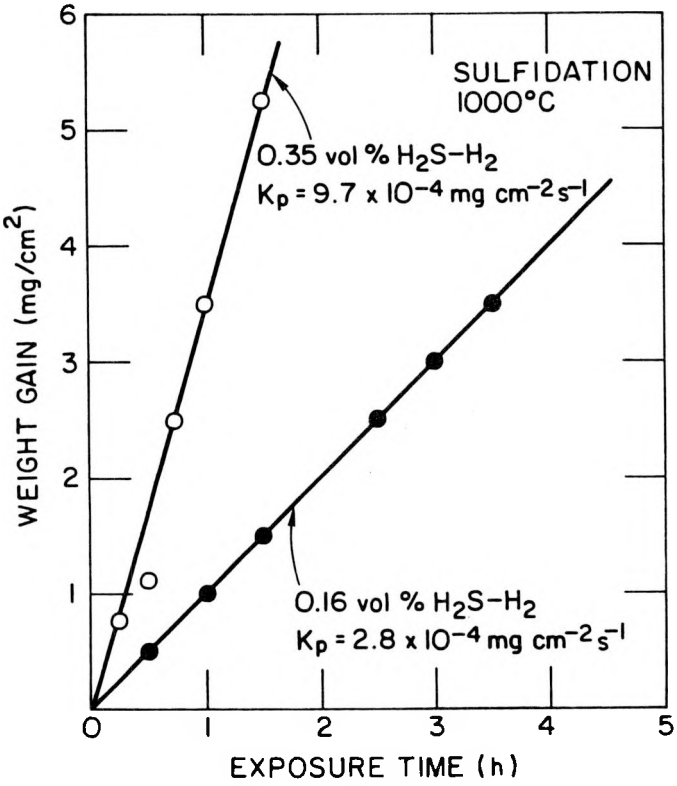

Fig. 14.
Thermogravimetric Test Data for Sulfidation of Bare ODS Alloy at 1000°C.

oxidation of the alloy. A listing of the linear rate constants obtained for the sulfidation of the bare and preoxidized alloy is included in Table 5.

Figure 15 shows weight gain versus time plots for sulfidation of preoxidized specimens of the alloy after exposure at 1000°C in several sulfur–containing atmospheres. The preoxidation treatment involved exposure of the specimens to 1 vol.% CO-CO_2 gas mixture at 1000°C for time periods of 40 to 65 h. The sulfidation period ranged from 6 to 20 h. The plots are linear and the weight gain data show an incubation time (during which the sulfidation rate was low) after which the rates increase. As the sulfur level increased to 1.35 vol.% H_2S, no incubation period was noted and sulfidation proceeded at a linear accelerated rate from the beginning of exposure.

Figure 16 shows weight change data for the oxidation of presulfidized alloy specimens at 1000°C. The presulfidation treatments were given for 1.5 h and 45 min in 0.35 and 0.16 vol.% H_2S-H_2 gas mixtures, respectively. The oxidation process seems to follow parabolic kinetics; however, at the 0.35 vol.% H_2S level of presulfidation, the subsequent rate of oxidation in CO-CO_2 was about two orders of magnitude higher than the oxidation rate observed in the absence of presulfidation. At the 0.16 vol.% H_2S level of presulfidation, the subsequent oxidation rate was affected much less when compared with that observed in the absence of presulfidation. Figure 17 shows a comparison of the weight change data obtained for the

Table 5. Values of Rate Constants for Sulfidation, Oxidation/ Sulfidation, and Sulfidation/Oxidation of ODS Alloy under Different Test Conditions

Exposure Condition	Temp. (°C)	Rate Constant (k_ℓ or k_p)
Bare Samples		
Sulfidation in $0.35H_2S$–H_2	1000	$k_\ell = 9.7 \times 10^{-4}$ mg cm^{-2} s^{-1}
Sulfidation in $0.16H_2S$–H_2	1000	$k_\ell = 2.8 \times 10^{-4}$ mg cm^{-2} s^{-1}
Preoxidized Samples		
Sulfidation in $0.16H_2S$–H_2	1000	$k_\ell = 2.2 \times 10^{-6}$, 2.8×10^{-5} mg cm^{-2} s^{-1}
Sulfidation in $0.35H_2S$–H_2	1000	$k_\ell = 4.6 \times 10^{-6}$, 6.9×10^{-5} mg cm^{-2} s^{-1}
Sulfidation in $1.35H_2S$–H_2	1000	$k_\ell = 1.7 \times 10^{-4}$ mg cm^{-2} s^{-1}
Sulfidation in $0.35H_2S$–H_2	650	$k_\ell = 1.8 \times 10^{-6}$, 7×10^{-7}mg cm^{-2} s^{-1}
Presulfidized Samples		
Sulfidation in $0.35H_2S$–H_2, Oxidation in CO–CO_2	1000	$k_p = 4.0 \times 10^{-4}$ mg^2 cm^{-4} s^{-1}
Sulfidation in $0.16H_2S$–H_2, Oxidation in CO–CO_2	1000	$k_p = 8 \times 10^{-7}$ mg^2 cm^{-4} s^{-1}

grit–blasted alloy specimen during oxidation in CO-CO_2-CH_4 gas mixture and sulfidation in 0.35 vol.% H_2S-H_2 gas mixture.

Morphology of Sulfidized, Preoxidized/Sulfidized, and Presulfidized/Oxidized Specimens

Figure 18 shows an SEM photograph and EDAX spectra for the alloy after sulfidation at 1000°C in 0.35 vol.% H_2S-H_2 gas mixture. The scale thickness was ~55 μm after only 2.5 h exposure to the sulfur–containing gas mixture. The scale was predominantly Cr sulfide, and very little aluminum was present. Further, the substrate alloy exhibited ~60–μm–deep penetration of internal sulfidation. Table 6 lists the reaction–product phases, identified by an X-ray diffraction technique, in several of the sulfidized, preoxidized/sulfidized, and presulfidized/oxidized specimens.

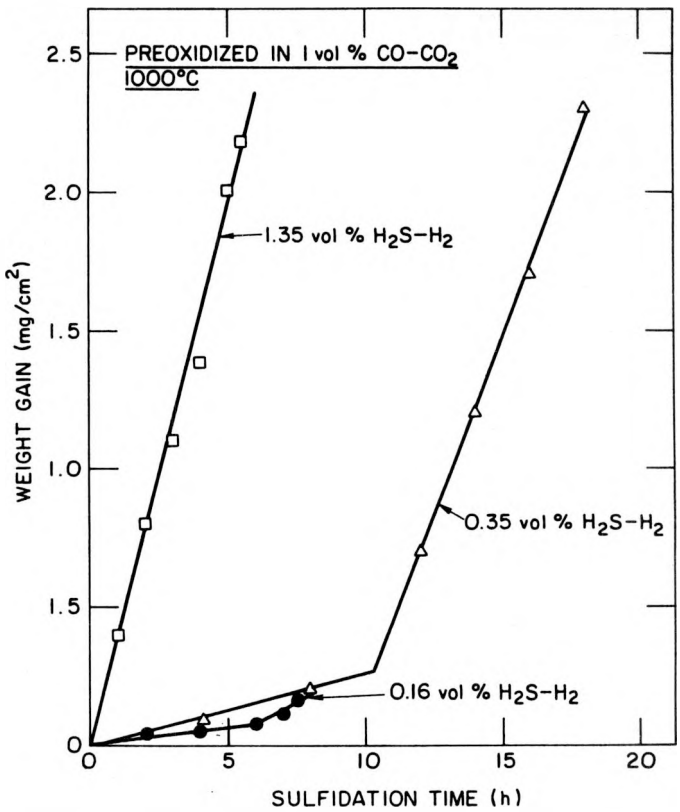

Fig. 15. Thermogravimetric Test Data for Sulfidation of Preoxidized ODS Alloy at 1000°C.

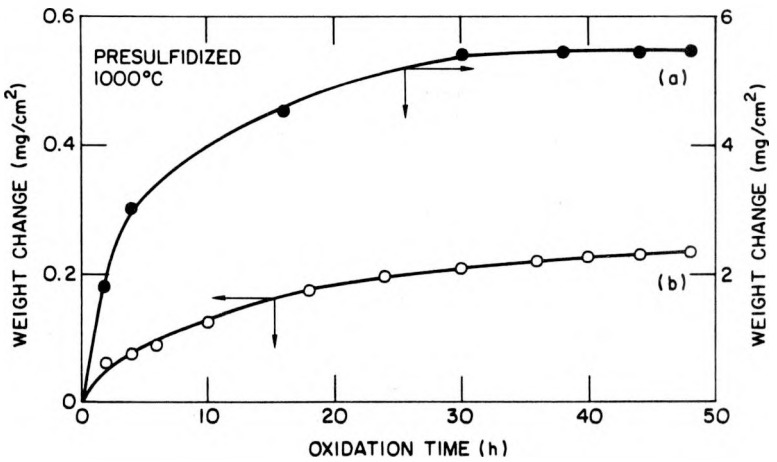

Fig. 16. Thermogravimetric Test Data for Oxidation of Presulfidized ODS Alloy at 1000°C.

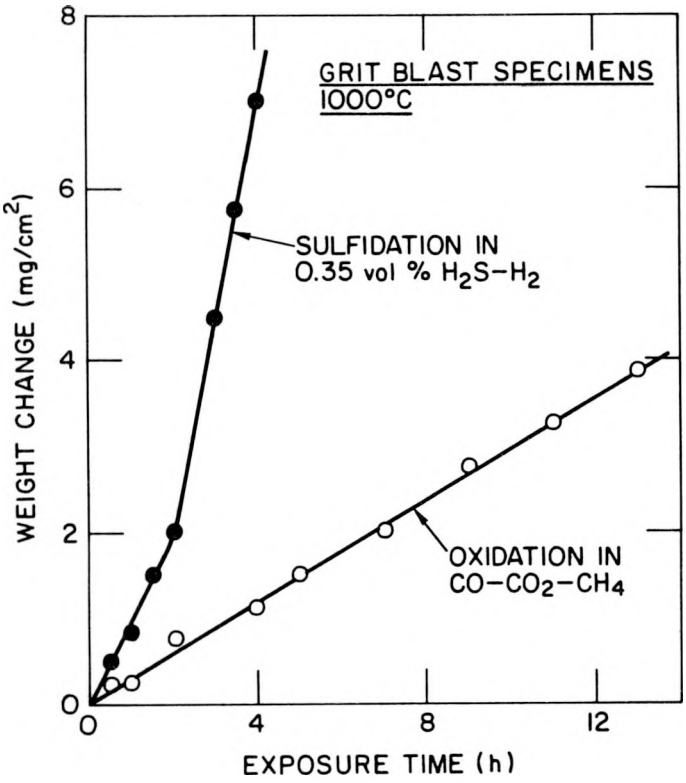

Fig. 17.
Comparison of Oxidation and Sulfidation Kinetics of Grit–Blasted ODS Alloy at 1000°C.

Figure 19 shows an SEM photograph and EDAX spectra for a specimen that was preoxidized and sulfidized at 1000°C. The specimen was preoxidized in 1 vol.% CO-CO_2 gas mixture for 40 h and sulfidized in 0.16 vol.% H_2S-H_2 gas mixture for 2.5 h. At 1000°C, the alumina scale that developed during preoxidation remained intact during the sulfidation step. In fact, very little, if any, sulfur was detected in either the scale or the substrate alloy at this temperature. EPMA analysis showed some redistribution of Y between the scale and the alloy substrate, but this did not seem to contribute towards sulfidation resistance of the scale. On the other hand, if the sulfidation step was carried out in a higher–sulfur environment (1.35 vol.% H_2S-H_2 gas), the oxide developed during the preoxidation step was completely destroyed and a massive sulfide scale ensued; this can be seen in the SEM photograph and elemental mapping for the exposed alloy in Fig. 20. Figure 21 is an SEM photograph of a grit–blasted specimen that was preoxidized and subsequently sulfidized in 0.35 vol.% H_2S-H_2 gas mixture at 1000°C. It was shown earlier that the grit–blasted specimen develops an external chromia scale during oxidation. This preoxidized layer is susceptible to sulfidation attack (see Fig. 21), and the extent and morphology of the sulfide layer are similar to those observed under direct sulfidation of the alloy (see Fig. 18).

Figure 22 shows an SEM photograph and EDAX spectra for a specimen that was preoxidized in 1 vol.% CO-CO_2 gas mixture for 131 h at 650°C and sulfidized at 650°C. The specimen developed an extremely thin scale (~0.1 μm) and offered very little resistance to sulfidation during the second step. As can be seen from Fig. 22,

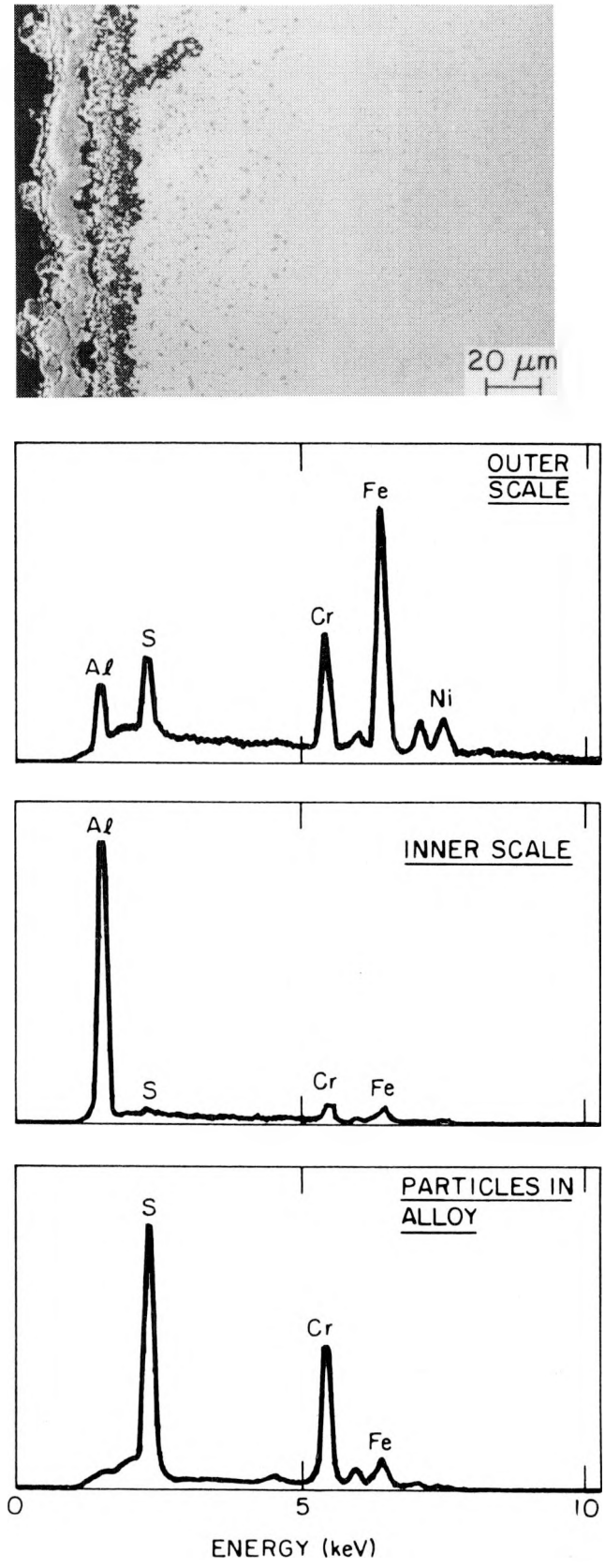

Fig. 18.
SEM Photograph and EDAX Spectra for ODS Alloy Sulfidized in 0.35 vol.% H_2S–H_2 Gas Mixture at 1000°C.

Table 6. X–Ray Diffractometer Analysis of ODS Alloy Specimens after Sulfidation, Oxidation/Sulfidation, and Sulfidation/Oxidation

Exposure Condition	Temp. (°C)	Reaction–Product Phases Identified	
		Major	Minor
Bare Samples			
Sulfidation in $0.35H_2S–H_2$	1000	Cr_2S_3, $NiCr_2S_4$, $FeCr_2S_4$	–
Preoxidized Samples			
Sulfidation in $0.16H_2S–H_2$	1200	Cr_2S_3, αAl_2O_3	–
Sulfidation in $0.16H_2S–H_2$	1000	Ni_3Al, αAl_2O_3	Cr_3S_4
Sulfidation in $0.35H_2S–H_2$	1000	Ni_3Al, Cr_3S_4, α, Al_2O_3	Cr_5S_6
Sulfidation in $0.35H_2S–H_2$	650	Cr_3S_4	$NiCr_2S_4$, Ni_3Al
Sulfidation[a] in $0.35H_2S–H_2$	1000	$NiCr_2S_4$, Cr_3S_4	–
Presulfidized Samples			
Sulfidation in $0.16H_2S–H_2$, Oxidation in $CO–CO_2$	1000	Cr_7S_8, Cr_2O_3	FeS, Ni_3Al
Sulfidation in $0.35H_2S–H_2$, Oxidation in $CO–CO_2$	1000	αAl_2O_3, Ni_3Al, Cr_7S_8	FeS

[a]Specimen was initially grit–blasted.

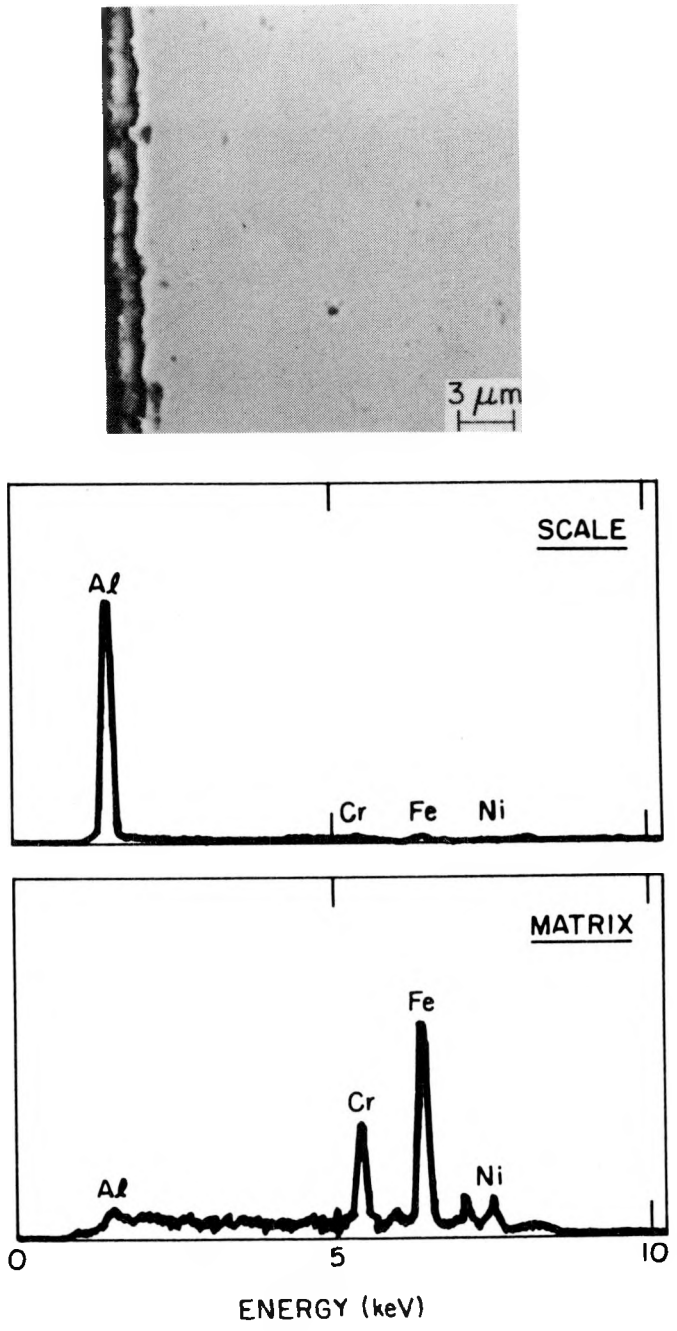

Fig. 19.
SEM Photograph and EDAX Spectra for Preoxidized Specimen Sulfidized in 0.16 vol.% H_2S–H_2 Gas Mixture at 1000°C.

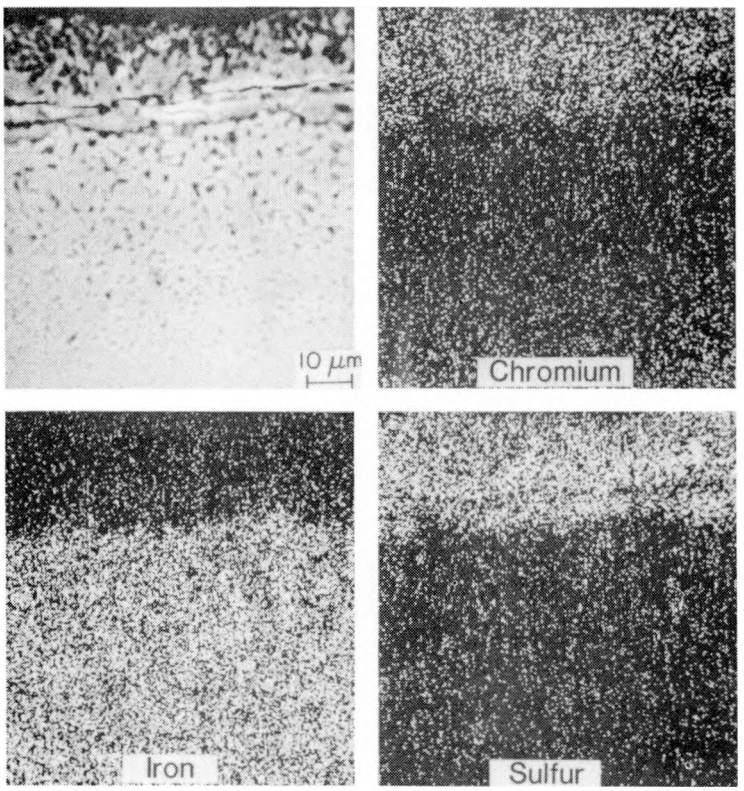

Fig. 20. SEM Photograph and Elemental Mapping for Preoxidized Specimen Sulfidized in 1.35 vol.% H_2S–H_2 Gas Mixture at 1000°C.

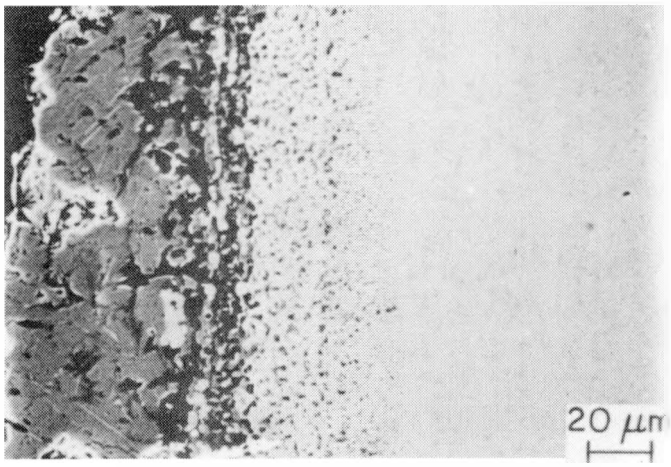

Fig. 21. SEM Photograph of Grit–Blasted Preoxidized Specimen Sulfidized in 0.35 vol.% H_2S–H_2 Gas Mixture at 1000°C.

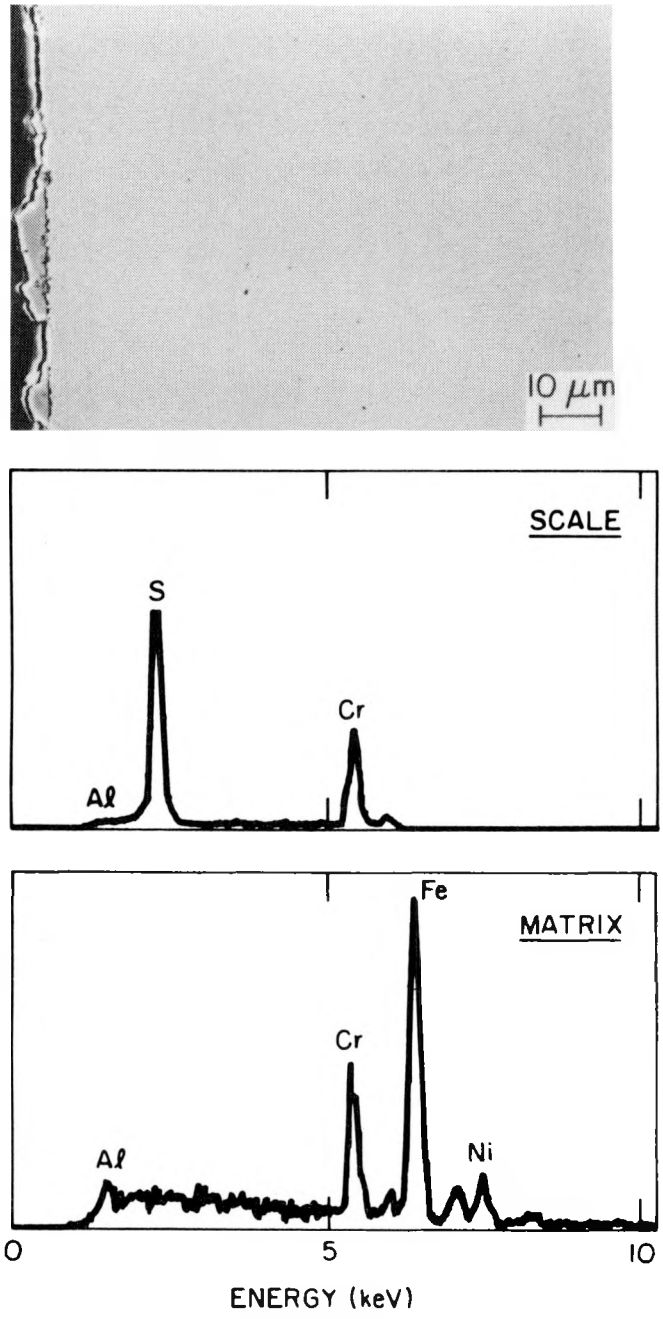

Fig. 22.
SEM Photograph and EDAX Spectra for Preoxidized Specimen Sulfidized at 650°C.

the external scale developed at this temperature was Cr sulfide, and no penetration of sulfur in the substrate was observed; however, due to the lower exposure temperature, the sulfide scale thickness was fairly small (~3 μm) after about 50 h of sulfidation treatment. Figure 23 shows an SEM photograph and EDAX spectra for corrosion product layers that developed on a specimen that was presulfidized and subsequently oxidized in a 1 vol.% CO-CO_2 environment at 1000°C. The presulfidation treatment was done in 0.35 vol.% H_2S-H_2 atmosphere for 1 h, while the oxidation step lasted 16 h. The figure shows that the outer scale was predominantly (Fe,Cr) sulfide, while an inner layer of alumina was formed; however, the protective ability of this oxide scale against further sulfidation of the alloy cannot be assessed.

Oxidation/Sulfidation in Oxygen/Sulfur Mixed Gas

Thus far, information was presented on the corrosion behavior of the ODS alloy exposed to a single oxidant, i. e., either an oxidizing or a sulfidizing gas mixture, and on the oxidation and sulfidation resistance of preformed scale layers. Experiments were also conducted to evaluate the corrosion behavior of the alloy in oxygen/sulfur mixed gas atmospheres. The exposure of an ODS alloy specimen to an environment with a simultaneous presence of both oxidizing and sulfidizing reactants leads to competition in the nucleation/growth of the oxide and sulfide phases during scale development, especially in the early stages of exposure. Depending on the relative values for the partial pressures of oxygen and sulfur, a sulfide scale can result even though oxide scale may be expected based on gas–phase equilibria and thermodynamic stability of the oxide and sulfide phases.

During the course of this work, two different oxygen/sulfur mixed gases were selected for the corrosion evaluation of the ODS material. Both mixtures established essentially the same oxygen partial pressure in the exposure environment, while sulfur partial pressures varied by a factor of ~20 between the two gas mixtures. Based on the earlier work, the gas chemistry established by mixture 2 probably represents the upper bound for the sulfur partial pressure in coal gasification systems that utilize a high–sulfur coal feedstock.[18,19] Figures 24 and 25 show weight change data for the ODS alloy after exposure in gas mixtures 1 and 2, respectively, at temperatures of 650, 871, and 1000°C. The data show that for given oxygen and sulfur partial pressures in the exposure environment, the corrosion rate of the alloy increases with an increase in temperature; also, at given exposure temperature, the corrosion rate of the alloy increases with an increase in sulfur partial pressure in the exposure atmosphere. For example, an increase in sulfur partial pressure by a factor of ~20 results in a six– to ninefold increase in weight change of the sample. In gas mixture 1, the alloy weight change seems to attain asymptotic values after ~60 h of exposure. On the other hand, the weight change of the samples exposed in mixture 2 seems to attain an asymptotic value only at 650°C, while it increases monotonically at 871 and 1000°C.

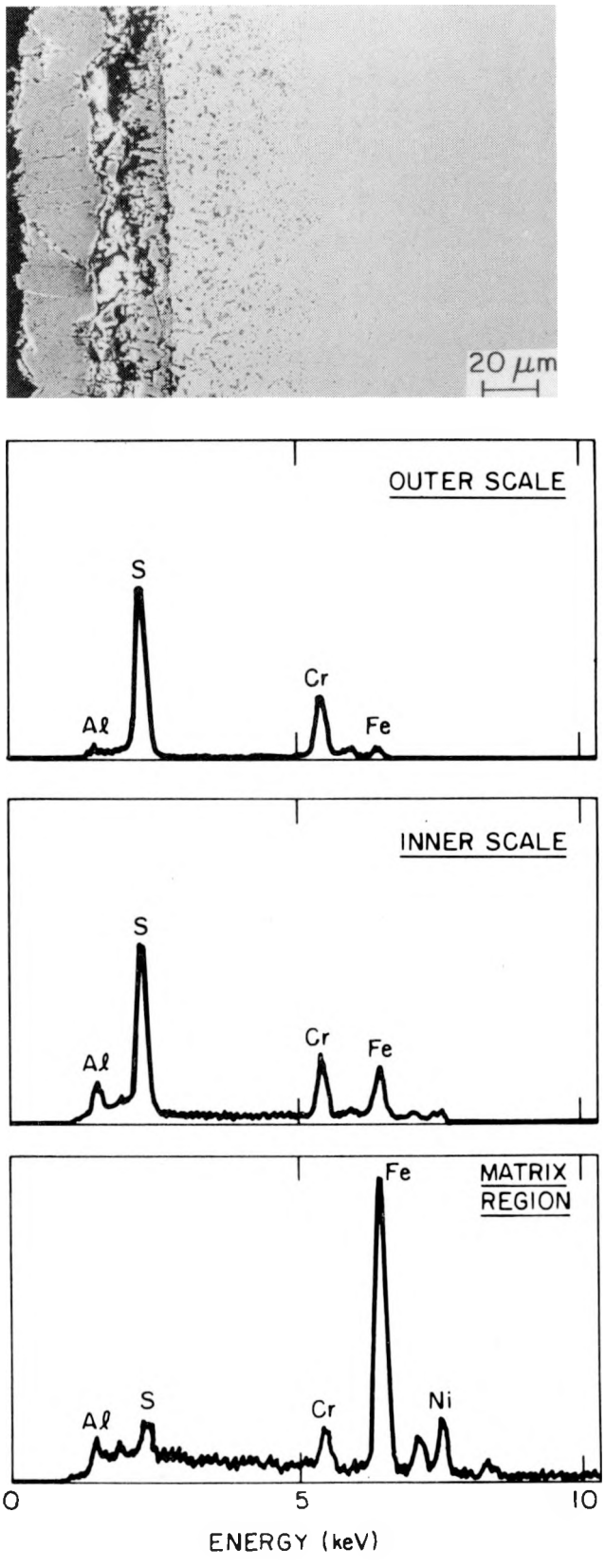

Fig. 23.
SEM Photograph and EDAX Spectra for Presulfidized Specimen Oxidized at 1000°C.

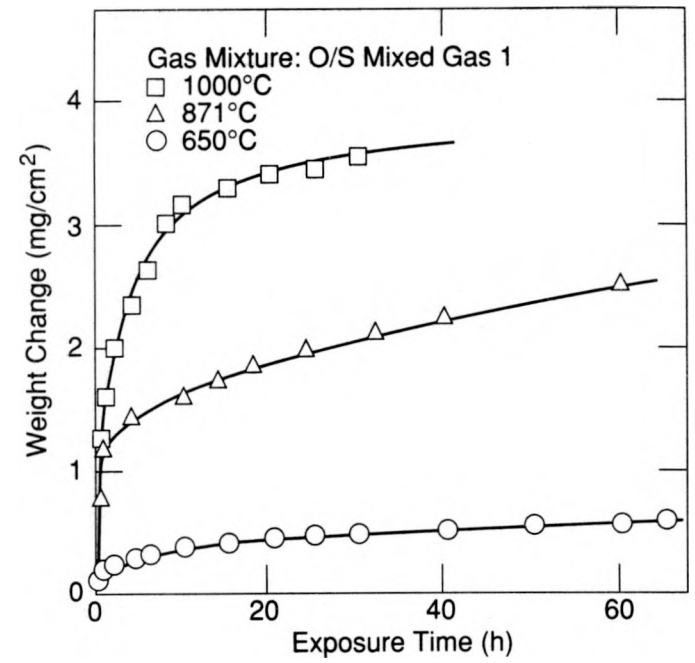

Fig. 24.
Thermogravimetric Test Data for ODS Alloy after Exposure at Several Temperatures to Oxygen/Sulfur Mixed Gas 1.

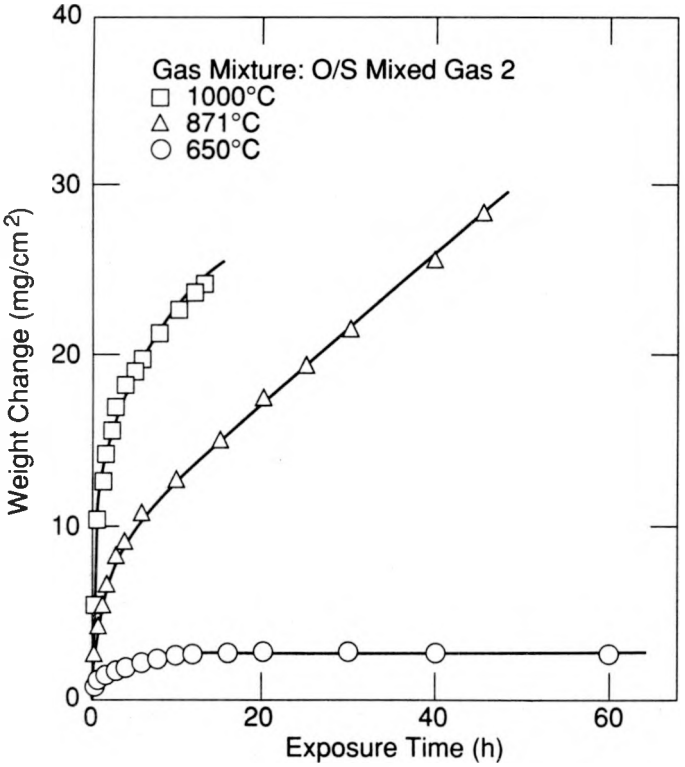

Fig. 25.
Thermogravimetric Test Data for ODS Alloy after Exposure at Several Temperatures to Oxygen/Sulfur Mixed Gas 2.

Figures 26–28 show SEM photographs of cross sections of samples of ODS alloy and Incoloy 800 after exposure to gas mixtures 1 and 2 at several temperatures. Incoloy 800 specimens were not tested at 1000°C because gross sulfidation attack of the alloy is expected at this temperature. In gas mixture 1, the ODS alloy developed a fairly thin (Cr,Fe) sulfide scale at 650 and 871°C, while it developed an (Fe,Cr) sulfide scale at 1000°C. An interesting feature in the morphology of the scale layer in these specimens is that the voids (that arose due to outward cation transport) were confined to the substrate alloy; virtually no void is noted at the scale/substrate interface. Even though the scales were of the sulfide type, there is an aluminum-enriched zone in the alloy below the scale that can act as a barrier to outward Cr and Fe migration, thereby lowering the corrosion rate for the alloy. The extent of aluminum enrichment at the interface region increased as the exposure temperature increased and in fact, aluminum-rich oxide was noted after 1000°C exposure. The presence of this oxide probably explains the lowering of the rate in the weight–change curves presented above. On the other hand, Incoloy 800 exposed under the same conditions developed substantially thicker (Fe,Cr) sulfide scales at 650 and 871°C. The outer scale spalled from the specimen exposed at 871°C. At both these temperatures, the Incoloy 800 specimens also developed an inner scale layer of (Cr,Fe) sulfide. Further into the specimen, substantial intergranular penetration of sulfur can be noted, especially at 871°C.

Upon exposure to gas mixture 2, the ODS alloy developed somewhat thicker (Fe,Cr) sulfide scales but as before, aluminum enrichment at the interface and voids in the substrate alloy were noted, especially at 650 and 871°C. At 1000°C, the alloy developed a Cr sulfide scale, and nodules of iron were rejected during the sulfidation process; however, a substantial internal sulfidation of the substrate alloy was observed. Specimens of Incoloy 800 exposed to the same gas mixture developed a somewhat thicker sulfide scale at 650°C but exhibited massive catastrophic sulfidation, which consumed the entire sample, at the exposure temperature of 871°C.

DISCUSSION

The oxidation kinetics of the ODS alloy Fe-20Cr-16Ni-4Al-1Y_2O_3 follow a parabolic rate law. This behavior is exhibited by the alloy in the temperature range of 650 to 1200°C in exposure environments of oxygen, air, and low-pO_2. The oxide scale in this alloy is fairly thin and has a composition of α-alumina. The parabolic rate constants for scale formation in this alloy are about two orders of magnitude lower than those for pure chromium.[21] For example, the values at 1000°C for the rate constant are 1.6×10^{-7} and 3.0×10^{-5} $mg^2\ cm^{-4}\ s^{-1}$ for the ODS alloy and pure chromium, respectively. In all oxidation experiments conducted in this study, the oxide scale was adherent to the substrate and no spallation of the oxide was noted on cooling to room temperature. The presence of Y seems to exert a positive influence on the growth and adherence of the oxide scales. The homogenized alloy contained

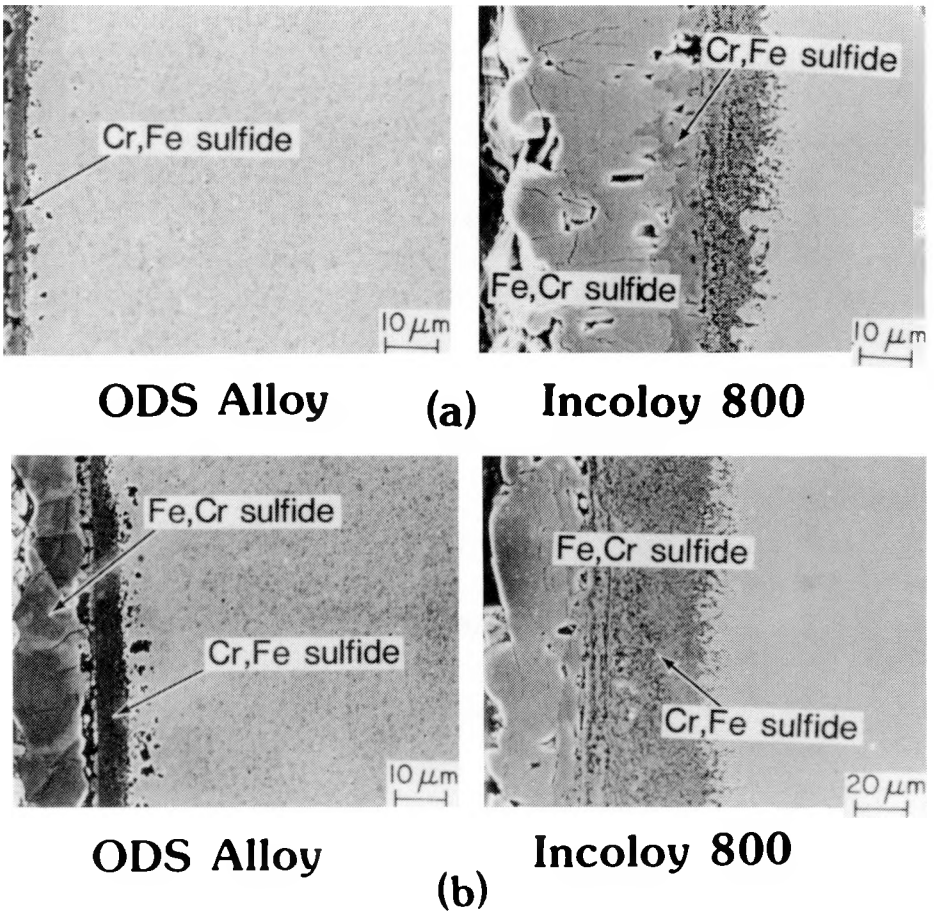

Fig. 26. SEM Photographs of Cross Sections of ODS Alloy and Incoloy 800 Specimens after Exposure at 650°C to Oxygen/Sulfur Mixed Gases: (a) Low pS_2 and (b) High pS_2.

a Y concentration of 0.8 wt.% in the form of Y_2O_3 dispersion and in solid solution in the matrix phase. During oxidation, Y_2O_3 particles are incorporated in the alumina scales, as evidenced by the EPMA results. The dispersoid Y2O3 promotes the development of an alumina scale either by incorporating into the scale itself or by forming a double oxide $Y_2O_3.M_2O_3$. This view is supported by the presence of Y in relatively higher concentrations at the alloy/scale interface in the oxidized samples. The development of fine–grained structure in Al_2O_3 scales is the consequence of Y_2O_3 dispersoids and is responsible for relief of oxide growth stresses by diffusional plastic flow.[16]

Nickel did not participate in the development of scale, even though ~16 wt.% Ni was present in the alloy; however, the presence of Ni and Al in the alloy led to fine precipitates of Ni3Al in the substrate alloy, as evidenced by the SEM photographs and X-ray diffraction data. At 650°C, alumina scale formed but its thickness

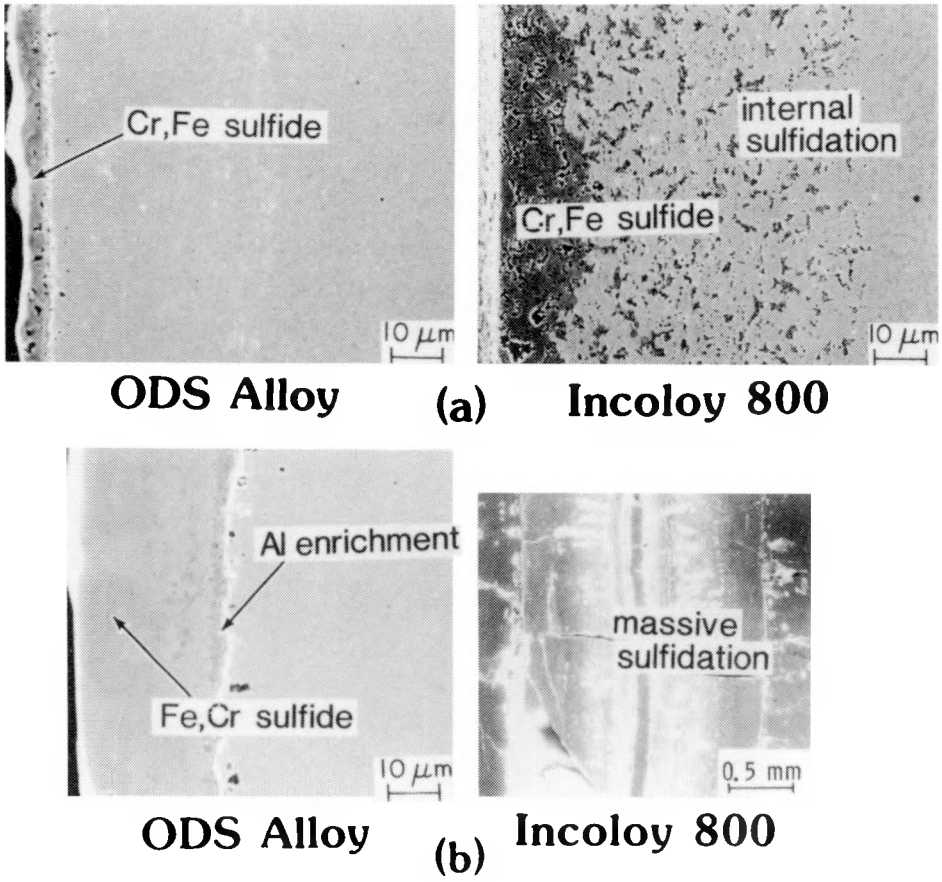

Fig. 27. SEM Photographs of Cross Sections of ODS Alloy and Incoloy 800 Specimens after Exposure at 871°C to Oxygen/Sulfur Mixed Gases: (a) Low pS_2 and (b) High pS_2.

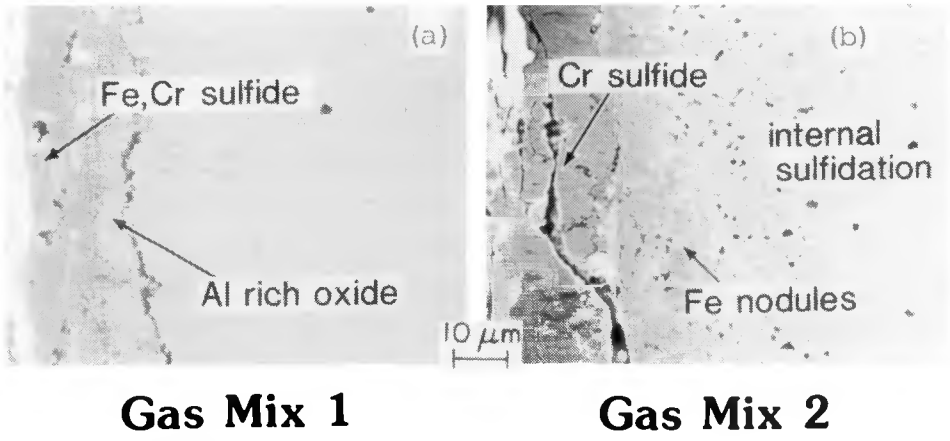

Fig. 28. SEM Photographs of Cross Sections of ODS Alloy Specimens after Exposure at 1000°C to Oxygen/Sulfur Mixed Gases: (a) Low pS_2 and (b) High pS_2.

was on the order of 0.1 μm after 130 h exposure; such a thin scale may not offer protection against sulfidation in sulfur–containing environments.

The sulfidation of the ODS alloy follows a linear rate law. Also, a linear relationship exists between the linear rate constant and the sulfur partial pressure in the exposure environment. X-ray diffraction analysis of the sulfide scales showed Cr_2S_3 as the dominant phase, along with some inclusions of spinel phase $FeCr_2S_4$. A Cr-depleted and Fe/Ni–enriched zone was observed in the alloy in the vicinity of the scale/alloy interface. The Cr-depleted zone formed due to the diffusion of Cr in forming the scale, therby creating a zone of metal vacancies that are eventually occupied by Fe and Ni ions.

The sulfidation of a preoxidized ODS alloy follows linear kinetics. In an environment of low sulfur partial pressure, the alloy shows an incubation period during which the rate is low. At 0.16 vol.% H_2S level, the alumina layer that developed during preoxidation was fairly intact and was resistant to internal sulfidation of the alloy. At higher sulfur partial pressures (e.g., 1.35 vol.% H_2S-H_2 mixture), the process followed linear kinetics with no incubation period. Under these conditions, the sulfidation of preoxidized ODS alloy resulted in thick outer scales of Cr sulfide containing inclusions of $FeCr_2S_4$. The original alumina scale was virtually destroyed. In addition, a Cr–depleted zone containing a dispersion of FeS particles was observed in the substrate below the scale/metal interface.

During oxidation of presulfidized alloy, the thick outer layer of Cr_2S_3 and $FeCrS_2$ (formed during the presulfidation step) remained intact. The sulfur released during oxidation of Cr_2S_3 led to sulfidation of aluminum diffused from the matrix and also resulted in internal sulfidation of the substrate alloy. The parabolic nature of the oxidation curves indicates that the process proceeds via diffusion of cations and anions.

The oxidation/sulfidation behavior of the ODS alloy exposed to oxygen/sulfur mixed gas environments is of particular interest in fossil energy systems because the component materials in these systems will be subjected to such environments in service. In this regard, an attempt has been made to compare the corrosion behavior of the present alloy with data developed earlier on several chromia- and alumina-forming alloys exposed to similar environments.[20] Among the alloys tested earlier, IN-792 and C-101 are nickel-base alloys with a composition of 12.7Cr-9Co-3.2Al-4.2Ti-2Mo-4Ta. In addition, C-101 alloy contains 1.1 wt.% Hf. These alloys, in general, form (Al,Ti) oxide scales when exposed to oxygen–containing environments at elevated temperature. Another alloy selected for comparison is an iron-base ODS alloy of the composition Fe-20Cr-4.5Al-0.5Ti-0.6Y_2O_3. Produced via mechanical alloying, this ODS alloy does not contain nickel and generally forms Al(Cr) oxide scale when exposed to oxidizing environments at elevated temperatures. In

addition, Incoloy 800 with a composition of Fe-21Cr-32.5Ni-0.4Al-0.4Ti, which forms a chromia scale, is included for comparison.

Figures 29 and 30 compare thermogravimetric data for several of the above–mentioned alloys at 871°C after exposure in oxygen/sulfur mixed gas atmospheres 1 and 2, respectively. The figures show Incoloy 800 to be the least resistant to sulfidation in these environments. The weight gains of 40 and 180 mg/cm^2 after ~25 h exposure to gas mixtures 1 and 2 can only be termed as catastrophic corrosion behavior. Alloys such as IN-792 and C-101 exhibited low rates of oxidation in gas mixture 1, and scale growth generally followed parabolic kinetics, indicating the protective nature of the scale. Alloy MA 956 developed a sulfide scale in gas mixture 1, but again the scaling process followed parabolic kinetics. The corrosion behavior of the present ODS alloy was similar to that of the Inconels, even though the scale in the ODS alloy was sulfide. The results from exposure in gas mixture 1 also show that the present ODS alloy with ~16 Ni exhibits no deleterious effects due to nickel presence, when compared with the behavior of MA 956, which contained no nickel.

The real contrast in the corrosion behavior of these alloys can be seen from the data in Fig. 30 for specimens exposed to gas mixture 2 with a higher sulfur partial pressure. The chromia-forming Incoloy 800 and the alumina-forming, high–nickel alloys IN-792 and C-101 exhibited catastrophic corrosion behavior. The weight change versus time curves were no longer parabolic but displayed accelerating corrosion rates with time to the point where the remaining surface area of uncorroded sample was so small that the rates based on the original surface area decreased. The commercial ODS alloy MA 956 (without Ni) and the present ODS alloy (with ~16Ni) exhibited parabolic scaling behavior, even though the scale itself was sulfide in both cases. As shown earlier, enrichment of Al at the scale/substrate interface region probably minimizes the base metal cation transport, thereby lowering corrosion rate. Nickel did not participate in the scaling process even at the (high sulfur partial pressure) anticipated–upper–bound value in practical systems established by gas mixture 2.

Figures 31 and 32 compare the corrosion behavior of Incoloy 800, MA 956, and the present ODS alloy at 650°C upon exposure to oxygen/sulfur gas mixtures 1 and 2, respectively. The results indicate protective scaling in the ODS alloys, with rates being at least one order of magnitude lower than those for Incoloy 800.

CONCLUSIONS

A mechanical alloying technique has been used to develop iron-base alumina-forming alloys that contained moderate concentrations of nickel and rare-earth metals or oxides. The Y_2O_3–containing ODS alloy developed in the present program has been

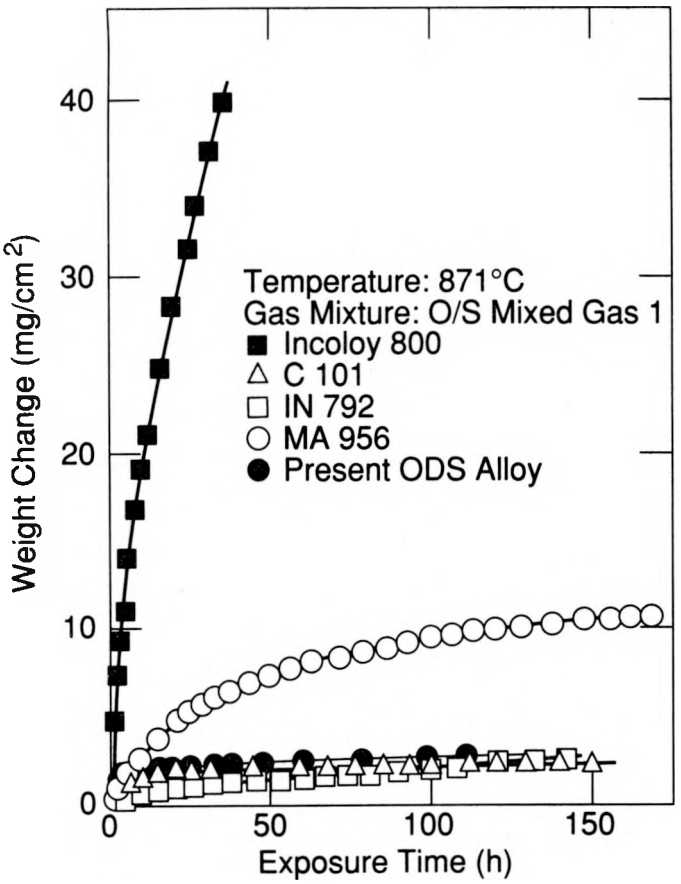

Fig. 29.
Comparison of Thermogravimetric Test Data for Several Alloys Tested at 871°C in Oxygen/Sulfur Mixed Gas 1.

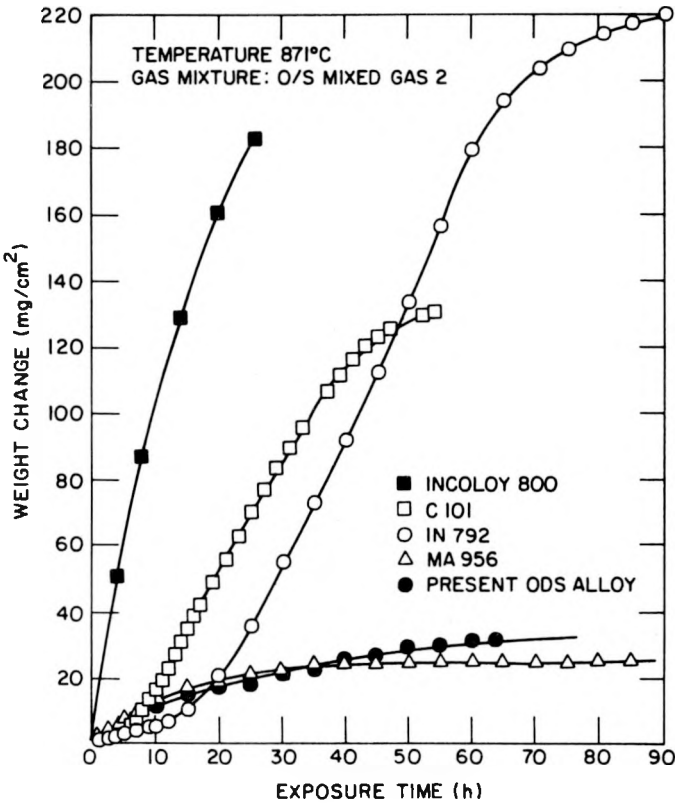

Fig. 30.
Comparison of Thermogravimetric Test Data for Several Alloys Tested at 871°C in Oxygen/Sulfur Mixed Gas 2.

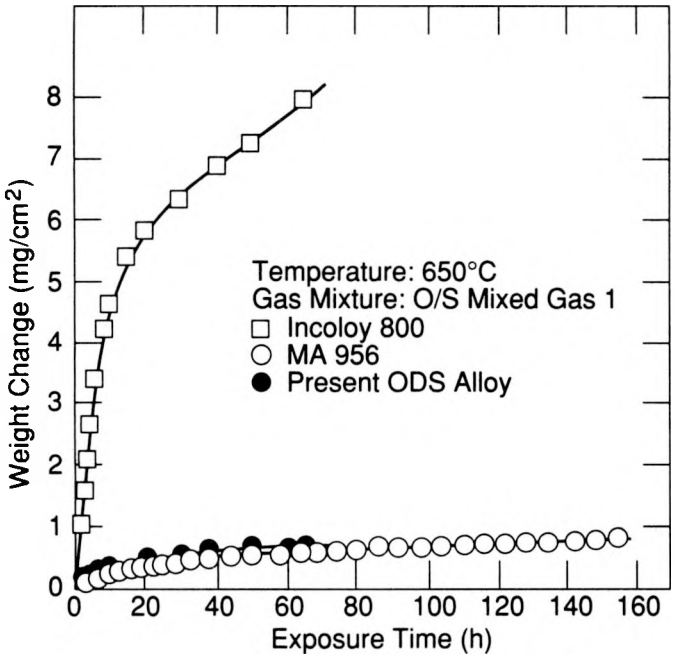

Fig. 31.
Comparison of Thermogravimetric Test Data for Several Alloys Tested at 650°C in Oxygen/Sulfur Mixed Gas 1.

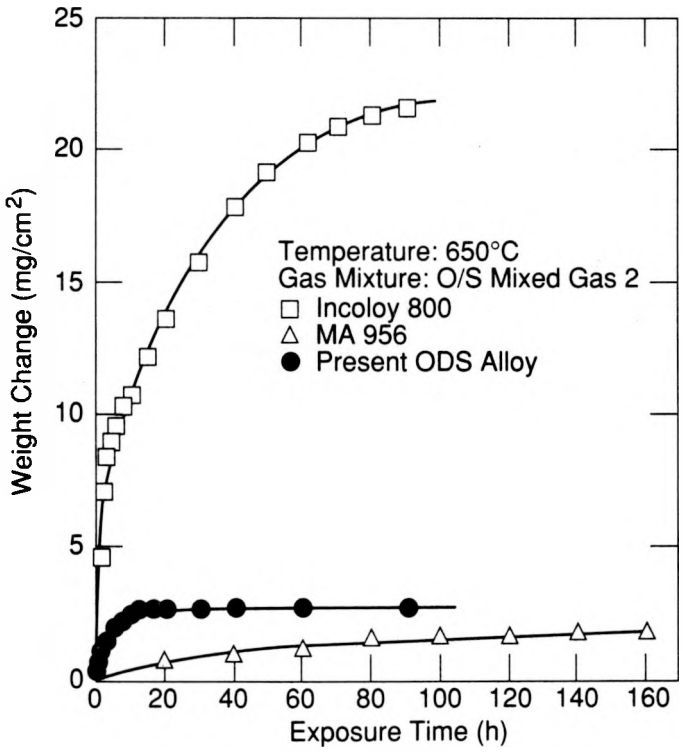

Fig. 32.
Comparison of Thermogravimetric Test Data for Several Alloys Tested at 650°C in Oxygen/Sulfur Mixed Gas 2.

examined for its oxidation and sulfidation behavior in oxidizing, sulfidizing, and oxygen/sulfur mixed gas atmospheres. Based on this study, a number of conclusions can be drawn:

1. The oxidation and sulfidation kinetics of the alloy follow parabolic and linear rate laws, respectively, over the temperature range of 650 to 1200°C. The primary scales developed during oxidation and sulfidation were alumina and (Cr,Fe) sulfide, respectively.

2. During sulfidation of preoxidized alloy specimens at 1000°C, the inner alumina layers remain protective at sulfur partial pressures below 10^{-6} atm, but break down at higher pressures.

3. Upon oxidation of a presulfidized alloy, the sulfur released during oxidation of the sulfide scales resulted in sulfidation of aluminum diffusing outward from the alloy substrate and to internal precipitation of Fe or (Fe,Cr) sulfides in the Al/Cr-depleted regions and in grain boundaries in the alloy.

4. The solute Y_2O_3 seems to promote the development of alumina scales either by incorporation into the scale itself or by formation of the double oxide $Y_2O_3.M_2O_3$.

5. A comparison has been made of the corrosion behavior of chromia-forming Incoloy 800, alumina-forming high–nickel alloys IN-792 and C-101, an Fe-base ODS alloy without nickel (MA 956), and the present ODS alloy containing ~16Ni. Thermogravimetric experiments conducted at 871°C in oxygen/sulfur environments with low levels of sulfur showed that the present alloy and the high–nickel alloys had comparably low corrosion rates. MA 956 had a higher rate but its kinetics followed a parabolic rate law. Incoloy 800 exhibited accelerated corrosion. Similar experiments conducted in high–sulfur environments showed catastrophic corrosion behavior for Incoloy 800, IN-792, and C-101 alloys, while a protective scaling kinetics was observed for MA 956 and the present ODS alloy. Even at 650°C and in a high–sulfur mixed gas atmosphere, the present alloy and MA 956 exhibited parabolic corrosion rates that were fairly low.

6. The present alloy contains ~16Ni and, coupled with Al, forms precipitates of Ni_3Al upon exposure to elevated temperatures. The presence of these precipitates, confirmed by X-ray diffraction analyses, should improve the strength properties of the alloy relative to those of nickel-free MA 956. Further, the presence of nickel in the present alloy did not result in any deleterious effect in the corrosion performance of the alloy (compared to that of MA 956) in air and sulfur-containing environments typical of fossil energy systems.

ACKNOWLEDGMENTS

The authors acknowledge the Fabrication Technology Section of the Materials and Components Technology Division at Argonne for its assistance in the fabrication of the alloy. D. L. Rink and R. W. Pucetti assisted in the thermogravimetric tests and microstructural analysis of the exposed specimens. Author A. U. Malik, who was a Fulbright Visiting Scholar at Argonne, is grateful for the financial support received from the Council for International Exchange of Scholars (CIES), USA, and from the University Grants Commission of the Government of India.

REFERENCES

1. R. E. Lawn, F. G. Wilson, and C. D. Desforges, *Oxide-dispersed Iron Alloys*, Powder Metallurgy, *19*, 196 (1976).

2. F. G. Wilson, B. R. Knott, and C. D. Desforges, *Preparation and Properties of Some ODS Fe-Cr-Al Alloys*, Met. Trans. *9A*, 275 (1978).

3. G. A. J. Hack, *Developments in the Production of Oxide Dispersion Strengthened Superalloys*, Powder Metallurgy, *27*, 73 (1984).

4. F. G. Wilson and C. D. Desforges, *Preparation and Properties of Some Advanced Oxide-dispersion Strengthened Alloys for High Temperature Use*, Proc. International Conf. on Behavior of High Temperature Alloys in Aggressive Environments, Oct. 15-18, 1979, Metal Society of London, 1017 (1979).

5. D. R. Tenney, C. T. Young, and H. W. Herring, *Oxidation Behavior of TD-NiCr in a Dynamic High Temperature Environment*, Met. Trans, *5*, 1001 (1974).

6. J. T. Stringer and I. G. Wright, *The High–Temperature Oxidation of Cobalt–2 wt.% Chromia–3 vol.% Y_2O_3 Alloys*, Oxid. Metals *5*, 59 (1972).

7. H. Nagai, S. Ishikawa, F. Koshi-isha, and K. Shoji, *High Temperature Oxidation of Ni–Cr Alloys with Disperson of Rare Earths and Other Reactive Metal Oxides and Their Doping Effect on the Electrical Conductivity of Cr_2O_3*, Proc. JIMIS-3 on High Temperature Corrosion of Metals and Alloys, Trans. Japan Inst. Metals, Supplement, 183 (1983).

8. P. Y. Hou and J. T. Stringer, *Effect of Surface Applied Reactive Element Oxides on the Oxidation of Cr–containing Binary Alloys*, Proc. Symp. on High Temperature Materials Chemistry III, Electrochemical Society, Las Vegas, *198* (1986).

9. K. L. Luthra and E. L. Hall, *High Temperature Oxidation of Ni–20Cr–12.5Al Coatings Containing 1% Dispersed Oxides*, Oxid. Metals, *26*, 385 (1986).

10. H. Nagai, Y. Takebayashi, and H. Mitani, *Effect of Dispersed Oxides of Rare Earths and Other Reactive Elements on the High Temperature Oxidation Resistance of Fe–20Cr Alloy*, Met. Trans. *12A*, 435 (1981).

11. T. Amano, S. Yajima, and Y. Saito, *High Temperature Oxidation of Fe–20Cr–4Al alloys with Small Additions of Sc, Y, or Er*, Proc. JIMIS-3 on High Temperature Corrosion of Metals and Alloys, Trans. Japan Inst. Metals, Supplement, 247 (1983).

12. J. C. Pevin, D. Delaunay, C. Roques-Carmes, A. M. Huntz, and P. Lacombe, *Oxidation Mechanism of Fe–Ni–20–25Cr–5Al Alloys – Influence of Small Amounts of Yttrium on Oxidation Kinetics and Oxide Adherence*, Corros. Sci. *20*, 351 (1980).

13. J. Peters and H. J. Grabke, *Formation of Alumina Layers on Iron–base Alloys*, Werkstoffe and Korrosion, *35*, 385 (1984).

14. D. P. Whittle and J. T. Stringer, *Improvement in Properties: Additives in Oxidation Resistance*, Phil. Trans. Royal Soc. London, *A 295*, 309 (1980).

15. H. Hindam and D. P. Whittle, *Mechanism of Peg Growth and Influence on Scale Adhesion*, Proc. JIMIS-3 on High Temperature Corrosion of Metals and Alloys, Trans. Japan Inst. Metals, Supplement, 261 (1983).

16. T. A. Ramanarayanan, M. Raghavan, and R. Petkovic-Luton, *The Characteristics of Alumina Scales Formed on Iron–based Yttria–dispersed Alloys*, J. Electrochemical Society, 131, 923 (1984).

17. J. G. Smeggil, A.W. Funkenbusch, and N.S. Bornstein, *A Relationship between Indigenous Impurity Elements and Protective Oxide Scale Adherence Characteristics*, Met. Trans, *17A*, 923 (1986).

18. K. Natesan, *Development of Oxide-dispersion Strengthened Alloys for Fossil Energy Applications*, Argonne National Laboratory Report ANL/FE-89/6 (October 1989).

19. T. C. Tiearney, Jr., and K. Natesan, *Metallic Corrosion in Simulated Low–Btu Coal–Gasification Atmospheres*, J. Materials for Energy Systems, *1*(4), 13 (1980).

20. T. C. Tiearney, Jr., and K. Natesan, *Sulfidation–Oxidation of Advanced Metallic Materials in Simulated Low–Btu Coal–Gasifier Environments*, Oxid. Metals, *17*(1/2), 2 (1982).

21. K. Natesan, *Alloy and Coating Development for Coal Gasification Applications*, Proc. Symp. Materials for Coal Gasification, ASM, Cincinnati (Oct. 10–15, 1987), eds. W. T. Bakker, S. Dapkunas, and V. Hill, ASM International, *137* (1988).

Distribution for ANL/FE–89/7

Internal:

H. Drucker
W. A. Ellingson
B. R. T. Frost
T. F. Kassner
C. A. Malefyt
K. Natesan (10)
J. H. Park
D. Schmalzer
W. J. Shack
C. E. Till
R. W. Weeks
ANL Patent Dept.
ANL Contract File
ANL Libraries
TIS Files (3)

External:

DOE–OSTI, for distribution per UC–114 (36)

DOE Chicago Operations Office:
H. J. Rauch F. Herbaty D. L. Bray

Materials and Components Technology Division Review Committee:
P. Alexander, Lord Corp., Erie, PA
M. S. Dresselhaus, Massachusetts Institute of Technology, Cambridge, MA
S. J. Green, Electric Power Research Institute, Palo Alto, CA
R. A. Greenkorn, Purdue U., West Lafayette, IN
L. Jardine, Lawrence Livermore Laboratory
C.-Y. Li, Cornell U., Ithaca, NY
R. E. Scholl, Counter Quake Corp., Redwood City, CA
P. G. Shewmon, Ohio State U., Columbus, OH
R. E. Smith, Electric Power Research Institute, N.D.E. Ctr., Charlotte, NC

U. S. Department of Energy, Washington:
Office of Fossil Energy:
D. J. Beecy J. P. Carr H. Feibus C. W. Garrett
F. Glaser P. Muchunas G. Rudins T. B. Simpson
Office of Conservation:
J. J. Brogan A. A. Chesnes J. J. Eberhardt
J. Eustis E. W. Gregory II M. E. Gunn, Jr.
Basic Energy Sciences, Materials Science Division
J. B. Darby

DOE Morgantown Energy Technology Center:
J. W. Byam J. E. Notestein

DOE Oak Ridge Operations Office:
Manager E. E. Hoffman

DOE Pittsburgh Energy Technology Center:

A. W. Deurbrouck J. D. Hickerson F. W. Steffen

Oak Ridge National Laboratory:

R. R. Judkins

Other Government – University – Industry:

D. R. Baer, Pacific Northwest Laboratory, Richland, WA
S. J. Dapkunas, National Institute of Standards and Technology, Gaithersburg, MD
D. Doughty, Sandia National Laboratories, Albuquerque, NM
V. L. Hill, Gas Research Institute, Chicago, IL
D. W. Keefer, EG&G IDAHO, Inc., Idaho National Engineering Laboratory, Idaho Falls, ID
A. V. Levy, Lawrence Berkeley Laboratory, Berkeley, CA
F. S. Pettit, University of Pittsburgh, Dept. of Materials Science and Engineering, Pittsburgh, PA
K. M. Prewo, United Technologies Research Center, East Hartford, CT
R. A. Rapp, Ohio State University, Columbus, OH
A. Schwanzkopf, National Science Foundation, Washington, D.C.
R. M. Spriggs, National Research Council, Washington, D.C.
V. Srinivasan, Universal Energy Systems, Inc., Dayton, OH
J. Stringer, Electric Power Research Institute, Palo Alto, CA
I. G. Wright, Battelle Columbus Laboratories, Columbus, OH
K. M. Zwilsky, National Materials Advisory Board, National Research Council, Washington, D.C.